Spin dynamics in anisotropic paramagnets

Charles W. Myles*
Laboratoire de Physique Expérimentale, Ecole Polytechnique Fédérale,† CH-1007 Lausanne, Switzerland
(Received 21 June 1976)

The spin dynamics of paramagnets with uniaxial and exchange anisotropy is investigated in the high-temperature limit. For a Hamiltonian consisting of both an anisotropic exchange and a uniaxial anisotropy interaction, lowest-order integral equations for the dynamical two-point correlation functions are derived by means of a previously developed infinite-temperature diagrammatic technique. These equations are valid for all values of the spin quantum number S and for all values of the ratio D/J, where D is the uniaxial anisotropy energy and J is an exchange energy. A systematic study of the numerical solutions to these equations is then made as a function of both S and $R = 3D^2/16S(S+1)J^2$ for $1 \leq S \leq 5/2$ and for $0.0 \leq R \leq 5.0$. In particular, the "local" spectral functions, the spin diffusion coefficients, and the exchange-narrowed dipolar linewidths are studied as a function of these parameters. The latter quantities are measurable in neutron scattering and EPR experiments in magnetic insulators. Finally, the diffusion coefficients and dipolar linewidths are evaluated for the uniaxial paramagnets NiF_2, CoF_2, FeF_2, and MnF_2, and the experimental implications of these results are discussed.

I. INTRODUCTION

The effects of a crystal-field anisotropy energy (i.e., single-ion anisotropy) on the static and thermodynamic properties of magnetic systems have received considerable attention in recent years.[1-8] Although an understanding of the effects of such a uniaxial anisotropy energy on the *dynamical* properties of paramagnets is very important for the explanation of such experiments as electron paramagnetic resonance,[9-13] Raman scattering,[14-17] and neutron scattering in magnetic insulators,[18] relatively little work appears to have been done in this area.

It should also be noted that a knowledge of the spin dynamics in paramagnetic systems is relevant to the understanding of the properties of other physical systems. For example, it has been shown that NMR experiments in solid ^{3}He can be described quite well using a Heisenberg model for the nuclear spins.[19-21]

Most of the existing theories of dynamical effects in anisotropic magnetic systems concentrate on effects either in the critical temperature regime[22-24] or in the low-temperature, spin-wave regime.[25-27] There have been a few treatments of the dynamics in the high-temperature, paramagnetic regime, but, until recently, these have usually been semiphenomenological[9] or moment method[28] approaches.

In the high-temperature regime, the only first-principles treatments of the dynamics of a paramagnet with uniaxial anisotropy to date has been the recent work of Joukoff-Piette and Resibois[29,30] (JPR). They have approached the problem with an infinite-temperature kinetic-equation formalism that is essentially an extension of earlier work by Resibois and Deleener[31] on the isotropic Heisenberg system. While their work is very elegant and is certainly a step in the right direction away from phenomenology, it is, unfortunately, so extremely formal as to obscure the physics of their approximations. Furthermore, their earlier papers[31] on the isotropic system have already been criticized[32] for predicting qualitatively incorrect fluctuation spectra at $T = \infty$, and it is not clear whether this defect has been corrected in JPR.

The first purpose of the present paper is to present an alternate formalism to that of JPR for the first-principles calculation of dynamical two-point correlation functions in a Heisenberg paramagnet with both anisotropic exchange and uniaxial (single ion) anisotropy. The formalism is based upon the technique of diagrammatically expanding the spin self-energy at infinite temperature. This technique is an extension of ideas due originally to Bennet and Martin.[33] These ideas were formulated in terms of moment diagrams by Reiter,[32] and were then expressed in terms of self-energy diagrams by Myles and Fedders.[34] The technique has previously been used successfully on a variety of different problems[34-39] and is capable, in principle, of diagrammatically generating equations for the self-energy which are valid to all orders of the interaction in a Brillouin-Wigner kind of perturbation theory. Although Fedders[40] has recently shown that, at least for the case of the isotropic Heisenberg magnet, it is possible to resume an infinite subset of these self-energy diagrams, in practice it is usually only practical to keep the lowest-order or "bubble" approximation in this diagrammatic expansion.[34-39] Because of the additional complexity of the problem with both ex-

change and uniaxial anisotropy included, in this paper only these lowest-order diagrams will again be kept. The resulting lowest-order integral equations give a formalism for the calculation of spin correlation functions which is applicable for all values of the spin quantum number S and for all values of the ratio D/J, where D and J are, respectively, the uniaxial anisotropy energy and an exchange energy. In addition, the correlation functions obtained by solving these equations are expected to contain errors of the order of $1/Z$, where Z is the number of spins[34-40] in the range of the interaction. These errors occur because the technique makes use of a high-density or $1/Z$ expansion to obtain and solve the basic equations.[34] In the last several years, such high-density expansions have been used by several authors[32,34,41,42] in conjunction with several different techniques to study various aspects of the physical properties of dense magnetic systems. The $1/Z$ expansion has, in fact, become a standard method for approximately treating problems in strongly interacting spin systems.

Although the equations resulting from this diagrammatic formalism and those given by JPR yield qualitatively similar numerical results, there are several advantages to the former approach over the latter. One advantage is that with the diagrammatic formalism, in contrast to the formalism JPR, one can obtain a clear recipe for extending the theory to higher orders in the interaction. The physics of such an extension is also clearer from the self-energy approach; one is making the extension by simply going to higher orders in a Brillouin-Wigner perturbation scheme. A second advantage of the method discussed below is that for a given value of S there are many less coupled integral equations to solve than with the method of JPR. Because of this fact, with the self-energy method, unlike the method of JPR, the introduction of a truncation scheme to reduce the number of equations for numerical solution is only necessary for large S. For example, by Eq. (2.16) of Ref. 30, for $S=\frac{5}{2}$ the formalism of JPR requires the simultaneous solution of 146 coupled integral equations.

Clearly, such a task is impractical for most computers, so that a truncation scheme must be introduced. On the other hand, using the formalism to be discussed below requires the solution of only 20 coupled integral equations for $S=\frac{5}{2}$, so that a computer solution without the introduction of a truncation scheme is still practical. A final advantage of the new formalism is that the diagrams used are not as complicated as those discussed by JPR so that the physical basis for the approximations made can hopefully be more easily seen.

As mentioned above, the application of the lowest-order or "bubble" approximation of the self-energy diagrammatic expansion to a paramagnet with anisotropic exchange and uniaxial anisotropy results in integral equations which are applicable for all values of the parameters S and D/J. The second purpose of the present paper is, in the limiting case of isotropic exchange, to make a systematic study of the numerical solutions to these equations as a function of both S and D/J. In particular, solutions for the "local" correlation functions, the spin-diffusion coefficients, and the exchange-narrowed dipolar linewidths will be studied as a function of S and R for $1 \leq S \leq \frac{5}{2}$ and $0.0 \leq R \leq 5.0$, where $R = 3D^2/16S(S+1)J^2$. The parameter R will be varied rather than D/J itself since R, as will be seen below, is a naturally occuring parameter in the equations for the correlation functions. Only the limiting case of isotropic exchange is considered for actual numerical study both for simplicity and because the main new features of the solutions, as compared to the case of the isotropic Heisenberg paramagnet, are expected to come from the uniaxial anisotropy rather than the anisotropic exchange.

The third and final purpose of this paper is to apply the above described formalism to real paramagnets with uniaxial anisotropy. In particular, the spin-diffusion coefficients and dipolar linewidths will be computed for the substances NiF_2, CoF_2, FeF_2, and MnF_2 and the experimental implications of these results will be discussed.

The remainder of this paper is organized as follows. Section II contains a discussion of the physical model to be used, the types of correlation functions to be considered and the notation to be used throughout the paper. In Sec. III, following a discussion of the spin self-energy method applied to the anisotropic Heisenberg paramagnet plus a uniaxial anisotropy energy, the lowest-order or "bubble" equations are derived for this system for all S. In Sec. IV, the method of solution to these equations is discussed and, in the limiting case of isotropic exchange, they are solved numerically for $1 \leq S \leq \frac{5}{2}$ and $0.0 \leq R \leq 5.0$. Sections V A and V B contain the calculations of the dependence of the spin-diffusion coefficients and exchange-narrowed dipolar linewidths on the parameters S and R. This dependence is computed using the self-consistent results of Sec. IV. In Sec. V C, the diffusion coefficients and dipolar linewidths are computed for the uniaxial paramagnets NiF_2, CoF_2, FeF_2, and MnF_2 and the relevance of these calculations to experiment is discussed. Finally, Sec. VI contains a brief summary and conclusions.

II. MODEL

It is assumed that the dynamics of the spins are adequately described by an anisotropic Heisenberg paramagnet plus a uniaxial anisotropy term. The Hamiltonian is then

$$H=-\tfrac{1}{2}\sum_{i,j\neq a,b} S_a(i)J_{ab}(i,j)S_b(j)-D\sum_i [S_z(i)]^2, \quad (1)$$

where $S_a(i)$ is the ath Cartesian component of the spin operator $\vec{S}(i)$ at site i which evolves in time according to the Heisenberg representation, $J_{ab}(i,j)=J_{ab}(i-j)$ is the exchange energy between spins at sites i and j, and D is the anisotropy energy. As is noted in Refs. 25 and 27, the physical origin of the anisotropy energy D in real paramagnets, such as MnF_2, is probably mainly the magnetic dipole-dipole interaction. For these real systems, then, it is probably more appropriate to replace the second term in Eq. (1) by the dipolar interaction or, equivalently, to absorb that dipolar interaction into the first term in that equation. On the other hand, the phenomenological parameter D is actually measured in several systems[43-47] so that if one uses Eq. (1) as it stands to calculate spin-correlation functions for realistic cases, experimental-theoretical comparisons of the results can be made by putting the measured value of D into the calculated results. Also, as stated above, one of the purposes of this paper is to investigate the dynamics of a *model* system described by Eq. (1). In particular, the dependence of the spin-correlation functions on the ratio D/J is one of the primary interests in the following calculations. Thus, the interaction will be taken in the phenomenological form of Eq. (1) with D (and, of course, the exchange energies) being taken as known. The effects of an external magnetic field could easily be included in the following discussion.[34,48] However, since for ordinary laboratory fields, the Zeeman interaction is only a small perturbation on H and since including this interaction would introduce many more indices into the notation, the effect of an external field will be neglected here.

Following Ref. 34, the two-point correlation functions to be considered here are defined in the high-temperature limit as

$$G_{\alpha\beta}(i,j,t-t')=\langle A_\alpha(i,t)A_\beta^\dagger(j,t')\rangle\Theta(t-t'), \quad (2)$$

where the angular brackets denote an average in the canonical ensemble, $\Theta(t)$ is a step function, and A_α is a shorthand notation for the irreducible tensor spin operator A_{lm}, where in general $-l \leq m \leq l$ and $l \leq 2S$. The operators A_{lm} are discussed and defined in Refs. 32 and 34 and are basically the Racah spherical harmonic operator equivalents discussed by Lindgärd and Danielsen[49] but with a change in normalization so that $\mathrm{Tr}(|A_{lm}|^2)=2S+1$. Table I of Ref. 49 gives a list of all Racah operator equivalents in terms of the ordinary spin operators $S_\pm, S_z$ for $0 \leq l \leq 8$. The precise method of obtaining the A_{lm} operators used here from the Racah operators is discussed in detail in Appendix A of the present paper. However, as will become apparent later, in order to obtain equations for the correlation functions it is not necessary to know the form A_{lm} take as a function of the spin operators. Rather, it is sufficient merely to know how these operators A_{lm} commute with one another. In this regard, as will be shown in detail in Appendix B, the commutation properties of the A_{lm} can be determined solely from their tensor properties without having to explicitly write the relationship between them and the spin operators. Thus, the reader is referred to Ref. 49 and Appendix A if he desires the detailed form of the A_{lm}.

The translational invariance of the system in time and the invariance of the crystal lattice under translations through a lattice vector enable one to Fourier transform $G_{\alpha\beta}(i,j,t-t')$ by the standard prescription[50]

$$G_{\alpha\beta}(i-j,t-t')=\frac{1}{N}\sum_{\vec{q}}\int_{-\infty}^{\infty}\frac{d\omega}{2\pi}G_{\alpha\beta}(\vec{q},\omega)e^{i\vec{q}\cdot(\vec{r}_i-\vec{r}_j)}e^{-i\omega(t-t')}, \quad (3)$$

where N is the number of lattice sites and the summation is over all wave vectors $\vec{q}$ in the first Brillouin zone. The Fourier-transformed function $G_{\alpha\beta}(\vec{q},\omega)$ is the function which will be of primary interest in the calculations to follow.

III. DERIVATION OF THE EQUATIONS OF MOTION

In this section, the diagrammatic method developed in Refs. 34 and 48 will be applied to the Hamiltonian, Eq. (1), to obtain equations of motion for the $G_{\alpha\beta}(\vec{q},\omega)$. Since it is basically the same method as was used for several previous calculations,[34-39] the following derivation will be as brief as possible with the main emphasis being on the features which are unique to the problem at hand. The starting point for the derivation is the expression of the correlation function in terms of a mass operator or self-energy $\Sigma_{\alpha\beta}(\vec{q},\omega)$. In the high-temperature limit, this function is defined by the equation

$$\omega G_{\alpha\beta}(\vec{q},\omega)-\Sigma_{\alpha\gamma}(\vec{q},\omega)G_{\gamma\beta}(\vec{q},\omega)=i\delta_{\alpha\beta}, \quad (4)$$

where γ is summed over and $\Sigma(t)$ is proportional to a step function. This definition of the mass operator is only useful, however, if one can find a method of expressing Σ as some functional of

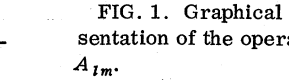

FIG. 1. Graphical representation of the operators A_{lm}.

the correlation function G.

In Refs. 34 and 48, it was shown rigorously that, for the isotropic Heisenberg paramagnet, such a functional can be obtained diagrammatically at infinite temperature. The method for proving the existance of such a diagrammatic expansion for $\Sigma_{\alpha\gamma}$ in the present case is exactly the same as was used in those references and the arguments which apply to the isotropic case apply equally well to the interaction given by Eq. (1). Thus, no detailed discussion of these points will be given here. In brief, then, the method for obtaining an infinite-temperature diagrammatic expansion of the self-energy is as follows. One first forms the Reiter-type moment diagrams[32] for the exchange plus uniaxial anisotropy interaction, Eq. (1). After keeping only the "skeleton diagram" [34] subset of these moment diagrams, diagrams for $\Sigma_{\alpha\gamma}$ are then obtained by resumming that subset by the same method as in Ref. 34.

Integral equations for $G_{\alpha\beta}$ can thus be obtained by the use of the Reiter-type vertices[32] from the interaction in Eq. (1). Since the equation of motion for A_{lm} couples to $A_{l+1,m}$ due to the commutation relation of A_{lm} with the second term of Eq. (1), in order to form vertices for that interaction it is necessary to include lines for the tensor operators A_{lm} for all $-l \leq m \leq l$ and for all $l \leq 2S$. Therefore, the graphical notation used in previous calculations,[34-39] where A_{lm} was represented by combinations of lines with arrows and dotted lines, would clearly be much too cumbersome for this case. Instead, the graphical representation for the tensor operator A_{lm} will be taken simply as a single line with the label (l,m). This notation is illustrated in Fig. 1.

Before forming the Reiter-type vertices[32] for the interaction of Eq. (1), it is convenient to first rewrite that interaction in terms of the tensor operators A_{lm}. The interaction then takes the form

$$H = -\tfrac{1}{6}S(S+1)\sum_{i,j;m,m'} A_{1m'}(i)J_{mm'}(i,j)A_{1m'}(j) - \mu_s D\sum_i A_{20}(i), \qquad (1')$$

where

$$\mu_s = [\tfrac{1}{45}S(S+1)(2S-1)(2S+3)]^{1/2}, \qquad (1'')$$

and an unimportant constant term has not been shown. The relationships between the exchange energies $J_{mm'}$ and the J_{ab} of Eq. (1) is shown explicitly in Appendix C.

The Reiter-type vertices[32] for the interaction Eq. (1') are formed from the matrix elements of the Liouville operator exactly as is discussed by Reiter.[32] The discussion here will be limited only to these basic vertices since they give all of the moments exactly to order $1/Z$, where Z is the number of spins in the range of the interaction. There are two kinds of these basic vertices which occur for the interaction of Eq. (1). The exchange interaction gives the usual kind[34-39] with one line entering the two lines leaving, while the uniaxial anisotropic interaction gives a vertex with one line entering and one line leaving. In the latter variety the interaction energy D will be denoted by a cross on the line. The Fourier-transformed basic vertices for the interaction of Eq. (1') are given, along with their analytical expressions, in Fig. 2. In that figure, the quantities $C^{lm'}_{l,m+m'}$ and $C^{20}_{l\pm1,m}$ are coefficients related to the commutators of the A_{lm} in the following manner:

$$[A_{1m'},A_{lm}] = C^{lm'}_{l,m+m'}A_{l,m+m'} \qquad (5a)$$

and

$$[A_{20},A_{lm}] = C^{20}_{l-1,m}A_{l-1,m} + C^{20}_{l+1,m}A_{l+1,m}. \qquad (5b)$$

In Sec. IV [Eqs. (10)], the explicit forms of these coefficients are shown for arbitrary S, l, and m and in Appendix B a detailed discussion is given

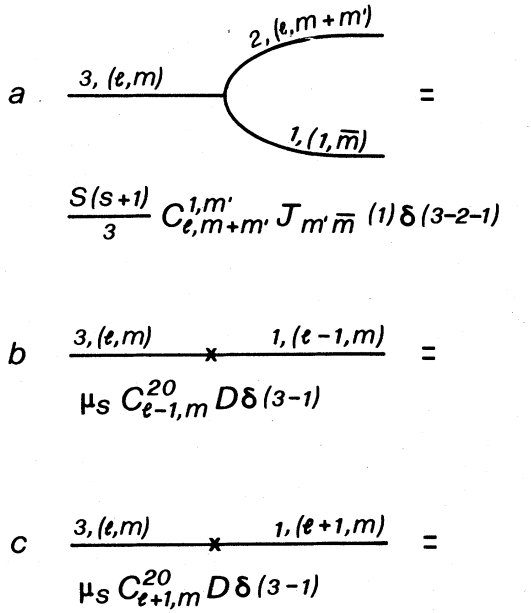

FIG. 2. Basic vertices for the interaction of Eq. (1') (a) Basic vertex for all l for the anisotropic exchange term. (b) Basic vertices for all l for the uniaxial anisotropy term. The shorthand, $\vec{q}_3 \equiv 3$, $\vec{q}_2 \equiv 2$, and $\vec{q}_1 \equiv 1$ has been used.

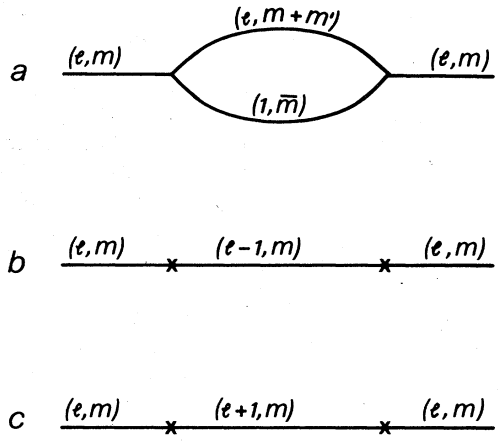

FIG. 3. Basic "bubble" diagrams. (a) Contribution of exchange; (b) and (c) contributions of uniaxial anisotropy.

on how one determines them, with particular emphasis on the derivation of the $C^{20}_{l\pm1,m}$. Curiously, the latter quantities do not appear to have been explicitly derived before.

For the infinite-temperature limit being considered here, only the diagonal correlation functions $G_{\alpha\alpha}$ and diagonal self-energies $\Sigma_{\alpha\alpha}$ are nonzero. Therefore, in the following discussion, the abbreviations $G_{\alpha\alpha}=G_{\alpha}=G_{lm}$ will be used with the corresponding abbreviations for the self-energy functions. Also, it should be noted that, in the absence of a magnetic field, $G_{lm}=G_{l,-m}$.

The vertices shown in Fig. 2 can be used to construct diagrams for Σ_{lm} which are valid to any order in the interaction. As was stated in the introduction, however, only the lowest order "bubble" approximation will be considered in this paper. The remainder of this paper will then be concerned with only this lowest-order approximation. These "bubble" diagrams are formed by connecting two of the vertices of Fig. 2. The basic types of these lowest-order diagrams are shown in Fig. 3. Note that, in this lowest-order approximation, there are no cross terms in Σ_{lm} between the energies $J_{mm'}$ and D. Evaluation of these diagrams by the rules discussed in Ref. 28 gives the following lowest-order self-energies:

$$\Sigma_{1m}(\vec{q},t)=\frac{iS^2(S+1)^2}{9N}\sum_{\vec{q}_1,\bar{m}m'}\{[J_{m'\bar{m}}(\vec{q}_1)]^2(C^{1,m'}_{1,m+m'})^2+J_{m'\bar{m}}(\vec{q}_1)J_{\bar{m}-m,m'+m}(\vec{q}-\vec{q}_1)C^{1,\bar{m}-m}_{1,\bar{m}}C^{1,m'}_{1,m+m'}\}$$
$$\times G_{1\bar{m}}(\vec{q}_1,t)G_{1,m+m'}(\vec{q}-\vec{q}_1,t)-i(\mu_s)^2D^2(C^{20}_{2+1,m})^2G_{2m}(\vec{q},t), \tag{6a}$$

$$\Sigma_{lm}(\vec{q},t)=\frac{iS^2(S+1)^2}{9N}\sum_{\vec{q}_1,\bar{m}m'}[J_{m'\bar{m}}(\vec{q}_1)]^2(C^{l,m'}_{l,m+m'})^2G_{1\bar{m}}(\vec{q}_1,t)G_{l,m+m'}(\vec{q}-\vec{q}_1,t)$$
$$-i(\mu_s)^2D^2[(C^{20}_{l-1,m})^2G_{l-1,m}(\vec{q},t)+(C^{20}_{l+1,m})^2G_{l+1,m}(\vec{q},t)],\ (1<l<2S), \tag{6b}$$

and

$$\Sigma_{2S,m}(\vec{q},t)=\frac{iS^2(S+1)^2}{9N}\sum_{\vec{q}_1,\bar{m}m'}[J_{m'\bar{m}}(\vec{q}_1)]^2(C^{1m'}_{2S,m+m'})^2G_{1\bar{m}}(\vec{q}_1,t)G_{2S,m+m'}(\vec{q}-\vec{q}_1,t)-i(\mu_s)^2D^2(C^{20}_{2S-1,m})^2G_{2S-1,m}(\vec{q},t). \tag{6c}$$

The second exchange energy term in Eq. 6(a) comes about because for $l=1$, there are two different ways of combining two vertices like the one in Fig. 2(a) to form the "bubble" in Fig. 3(a). Equation (6c) is clearly a special case of Eq. (6b) but it has been written to emphasize the fact that the hierarchy of equations truncates automatically at $l=2S$ because of the properties of the coefficients $C^{20}_{l+1,m}$. In particular, as can be seen from Sec. IV and Appendix B, $C^{20}_{2S+1,m}$ is identically zero. Likewise, $C^{20}_{1-1,m}$ vanishes and there is only one term in Eq. (6a) which is proportional to D^2. Thus, it can be seen that the present formalism, when the symmetry in m and $-m$ due to the absence of an external field is taken into account, requires the simultaneous solution, for a given S, of

$$\sum_{l=1}^{2S}(l+1)=S(2S+1)+2S=S(2S+3)$$

coupled nonlinear integral equations. This should be compared with the formalism of JPR which requires[29] the simultaneous solution of $\frac{1}{3}(2S+1)[8S(S+1)+3]$ such equations for a given S. For the present formalism, it has been found that a numerical solution without the introduction of an artificial truncation scheme is practical even for S as high as $\frac{5}{2}$. On the other hand, the JPR formalism requires, from a practical point of view, the introduction of such a truncation scheme for any S. For very large S, a truncation scheme is probably also necessary with the present formalism and a method similar so that used by JPR would probably be applicable.

As can be seen from Appendix B, the quantities $C^{1m'}_{l,m+m'}$ are of the form

$$C^{1m'}_{l,m+m'}=[3/S(S+1)]^{1/2}b^{1m'}_{l,m+m'},$$

where the $b^{1m'}_{l,m+m'}$ are independent of S and are shown explicitly in that appendix and in Eq. (10a) of Sec. IV. Thus, the S dependence of the exchange terms of Eqs. (6) consists merely of the scale factor

$$\tfrac{1}{9}S^2(S+1)^2\{[3/S(S+1)]^{1/2}\}^2=\tfrac{1}{3}S(S+1).$$

This is in agreement with previous results for the isotropic Heisenberg system.[34,48] On the other hand, the quantities $C^{20}_{l\pm1,m'}$ and thus the terms in Eqs. (6) which are proportional to D^2, have a more complicated S dependence. This dependence is shown explicitly in Eqs. (10b) and (10c) and may be found from the forms of $C^{20}_{l\pm1,m}$ which are derived in Appendix B.

Equations (6a)–(6c) along with Eq. (4) form a closed set of nonlinear integral equations for the correlation functions G_{lm}. These equations reproduce the infinite-temperature frequency moments of the Σ_{lm} exactly to lowest order in $1/Z$. While only valid for infinite temperature, they are also valid for all values of the spin quantum number S, for arbitrary ratios of the uniaxial anisotropy energy to the exchange energy, and for arbitrary exchange anisotropy. Furthermore, they are the lowest-order equations in a Brillouin-Wigner perturbation theory in the energies $J_{mm'}$ and D. The exchange-energy–dependent part of Eq. (6a) has been obtained before in a slightly different notation.[34,48,51] Also, the exchange-dependent part of Eq. (6b) has been obtained before for the limiting case of $l=2$ and isotropic exchange.[34] However, the derivation of these equations for general l,m and the inclusion of uniaxial anisotropy effects are new results.

IV. SOLUTION OF EQUATIONS FOR THE CASE OF ISOTROPIC EXCHANGE

In this section, the nonlinear integral equations derived in Sec. III will be solved for the limiting case of isotropic exchange for $1\leq S\leq\frac{5}{2}$, and for various ratios D/J of uniaxial anisotropy and exchange energies. Only the limiting case of isotropic exchange is considered both for reasons of numerical simplicity and because the uniaxial anisotropy energy should reasonably be expected to produce the most significant new features of the solutions for the correlation functions, as compared to the solutions for the isotropic case discussed in Ref. 34. In Sec. V, the solutions for the dipole correlation functions $G_{lm}(\vec{q},\omega)$ will be used to obtain the spin-diffusion coefficients and exchange-narrowed dipolar linewidths as a function of S and D/J.

First, for convenience, the G_α and the Σ_α are expressed in terms of spectral representations as

$$G_\alpha(\vec{q},\omega)=i\int_\infty^\infty\frac{d\omega'}{\pi}\frac{g_\alpha(\vec{q},\omega')}{\omega-\omega'+i\epsilon} \tag{7a}$$

and

$$\Sigma_\alpha(\vec{q},\omega)=\int_{-\infty}^{\infty}\frac{d\omega'}{\pi}\frac{\Gamma_\alpha(\vec{q},\omega')}{\omega-\omega'+i\epsilon}$$
$$=\Pi_\alpha(\vec{q},\omega)-i\Gamma_\alpha(\vec{q},\omega) \tag{7b}$$

where ϵ is a positive infinitesimal quantity. The quantity $g_\alpha(\vec{q},\omega)$ is the experimentally measured line-shape function and is related to $\Pi_\alpha(\vec{q},\omega)$ and $\Gamma_\alpha(\vec{q},\omega)$ by the equation

$$g_\alpha(\vec{q},\omega)=\Gamma_\alpha(\vec{q},\omega)/\{[\omega-\Pi_\alpha(\vec{q},\omega)]^2+[\Gamma_\alpha(\vec{q},\omega)]^2\}. \tag{8}$$

By Fourier transforming Eqs. (6a)–(6c), and by using the above spectral function definitions, it can be seen that, in the isotropic exchange limit, those equations are equivalent to

$$\Gamma_{1m}(\vec{q},\omega)=\frac{S(S+1)}{3N}\sum_{\vec{q}_1}\{[J(\vec{q}_1)]^2-J(\vec{q}_1)J(\vec{q}-\vec{q}_1)\}\sum_{m'}(b^{1,m'}_{1,m+m'})^2\int_{-\infty}^{\infty}\frac{d\omega_1}{\pi}g_{1,-m'}(\vec{q}_1,\omega_1)g_{1,m+m'}(\vec{q}-\vec{q}_1,\omega-\omega_1)$$
$$+D^2[d^{20}_{2,m}(S)]^2g_{2m}(\vec{q},\omega), \tag{9a}$$

$$\Gamma_{lm}(\vec{q},\omega)=\frac{S(S+1)}{3N}\sum_{\vec{q}_1}[J(\vec{q}_1)]^2\sum_{m'}(b^{1,m'}_{l,m+m'})^2\int_{-\infty}^{\infty}\frac{d\omega_1}{\pi}g_{1,-m'}(\vec{q}_1,\omega_1)g_{l,m+m'}(\vec{q}-\vec{q}_1,\omega-\omega_1)$$
$$+D^2\{[d^{20}_{l-1,m}(S)]^2g_{l-1,m}(\vec{q},\omega)+[d^{20}_{l+1,m}(S)]^2g_{l+1,m}(\vec{q},\omega)\},\quad(1<l<2S), \tag{9b}$$

and

$$\Gamma_{2S,m}(\vec{q},\omega)=\frac{S(S+1)}{3N}\sum_{\vec{q}_1,m'}[J(\vec{q}_1)]^2(b^{1,m'}_{2S,m+m'})^2\int_{-\infty}^{\infty}\frac{d\omega_1}{\pi}g_{1,-m'}(\vec{q}_1,\omega_1)g_{2S,m+m'}(\vec{q}-\vec{q}_1,\omega-\omega_1)$$
$$+D^2[d^{20}_{2S-1}(S)]^2g_{2S-1,m}(\vec{q},\omega). \tag{9c}$$

Note that to obtain Eqs. (9) from Eqs. (6) use has been made of the fact that, in the isotropic exchange

limit, $J_{m',\bar{m}} = \delta_{m',\bar{m}} J$. In Eqs. (9) the quantities $b^{1;m'}_{l;m+m'}$ and $d^{20}_{l\pm1,m}(S)$ have been introduced, where

$$(b^{1,m'}_{l,m+m'})^2 \equiv \tfrac{1}{3}S(S+1)(C^{1,m'}_{l,m+m'})^2 = \begin{cases} \tfrac{1}{2}[l(l+1) - m(m\pm1)], & m' = \pm 1, \\ m^2, & m' = 0, \\ 0, & \text{otherwise}, \end{cases} \tag{10a}$$

$$[d^{20}_{l+1,m}(S)]^2 \equiv (\mu_s)^2 (C^{20}_{l+1,m})^2 = \frac{m^2(l+m+1)(l-m+1)[4S(S+1) - l(l+2)]}{(2l+1)(2l+3)}, \tag{10b}$$

and

$$[d^{20}_{l-1,m}(S)]^2 \equiv (\mu_s)^2 (C^{20}_{l-1,m})^2 = \frac{m^2(l+m)(l-m)[4S(S+1) - (l-1)(l+1)]}{(2l-1)(2l+1)}. \tag{10c}$$

Here, explicit use has been made of the definitions of $C^{1,m'}_{l,m+m'}$ and $C^{20}_{l\pm1,m}$ derived in Appendix B and, for emphasis, the $d^{20}_{l\pm1,m}(S)$ have been written explicitly as functions of S.

Equations (8) and (9a)–(9c) are the integral equations which will be discussed in this section. Solving these sets of four variable nonlinear integral equations could be very difficult in the general case. Thus, following Refs. 34–39, the "local" equations will be solved first and the self-consistent solutions to these equations (the "local" spectral functions) will be substituted into Eqs. (9) to obtain an approximation to the wave-vector–dependent linewidth functions $\Gamma_{lm}(\vec{q}, \omega)$. In particular, the "local" solutions for the dipolar spectral functions g_{lm} will be used to obtain approximations to the functions $\Gamma_{1m}(\vec{q}, \omega)$ which can be used to calculate the spin-diffusion coefficients and the dipolar linewidths.

The philosophy behind making such a "local" approximation to Eqs. (9) has been thoroughly discussed in Refs. 34 and 48, where it is given a rigorous mathematical foundation. Thus, here only the main ideas which form the basis for this approximation will be discussed. The approximation is based on the fact that Eqs. (9), which are the result of the "bubble" approximation to the self-energy, are only accurate to order $1/Z$, since they are the analytic representation of diagrams formed from vertices which only give the moments accurately to that order. Thus, if these equations are themselves expanded to lowest order in $1/Z$, one would expect the solutions of the resulting equations to be almost as accurate as the solutions to the exact equations. Such an expansion of Eqs. (9) is known as the "local" approximation. It should be emphasized that this local approximation is not a necessary approximation to solve Eqs. (9). It is, however, an approximation which makes the numerical solution to those equations much easier and more economical with respect to the amount of computer time used, while at the same time, it sacrifices very little in accuracy as compared to an exact solution. In particular, physically observable quantities which are calculated from the approximate solutions are expected to differ by only one or two percent from the values that would be obtained if the exact solutions were used. This expectation has previously been confirmed quantitatively for the case of the isotropic Heisenberg magnet by comparing the electronic spin-diffusion coefficients[34] and the NMR linewidths[35] computed using solutions to the "local" approximation equations to those same quantities computed using Blume and Hubbard's[52] exact solutions for that case. Finally, it should be noted that the approximation just discussed has the effect, in coordinate space, of replacing $g_\alpha(i,j,\omega)$ by $g_\alpha(\omega)\delta_{i,j}$. The functions $g_\alpha(\omega)$ are thus the spectral functions for the autocorrelation functions and the physical origin of the term "local" approximation can be seen.

In the following discussion, it will be convenient to use dimensionless variables so that frequencies are measured relative to V, where

$$V^2 = \frac{2S(S+1)}{3N}\sum_{\vec{q}} J^2(\vec{q}). \tag{11}$$

Thus, the dimensionless variables here and those in Ref. 34 are the same, which will facilitate comparison of the results obtained here with those obtained for the isotropic case. It can be shown that expanding Eqs. (9) in the manner discussed above leads to the following wave-vector–independent equations:

$$\tilde{\Gamma}_{1m}(y) = \tfrac{1}{2}\sum_{m'} (b^{1,m'}_{1,m+m'})^2 \int_{-\infty}^{\infty} \frac{dy_1}{\pi} \tilde{g}_{1,-m'}(y_1)\tilde{g}_{1,m+m'}(y-y_1) + R[d^{20}_{2,m}(S)]^2 \tilde{g}_{2m}(y), \tag{12a}$$

$$\tilde{\Gamma}_{lm}(y)=\tfrac{1}{2}\sum_{m'}(b^{1,m'}_{l,m+m'})^2\int_{\infty}^{\infty}\frac{dy_1}{\pi}\tilde{g}_{1,-m'}(y_1)\tilde{g}_{l,m+m'}(y-y_1)$$
$$+R\{[d^{20}_{l-1,m}(S)]^2\tilde{g}_{l-1,m}(y)+[d^{20}_{l+1,m}(S)]^2\tilde{g}_{l+1,m}(y)\},\ (1<l<2S), \tag{12b}$$

and

$$\tilde{\Gamma}_{2S,m}(y)=\tfrac{1}{2}\sum_{m'}(b^{1,m'}_{2S,m+m'})^2\int_{-\infty}^{\infty}\frac{dy_1}{\pi}\tilde{g}_{1,-m'}(y_1)\tilde{g}_{2S,m+m'}(y-y_1)+R[d^{20}_{2S-1,m}(S)]^2\tilde{g}_{2S-1,m}(y). \tag{12c}$$

where $y=\omega/V$ is a dimensionless frequency, $R=D^2/V^2$, and the tilde denotes that the quantities are in dimensionless form. Similarly, the dimensionless "local" forms of Eqs. (8) and (7b) are

$$\tilde{g}_{\alpha}(y)=\tilde{\Gamma}_{\alpha}(y)/\{[y-\tilde{\Pi}_{\alpha}(y)]^2+[\tilde{\Gamma}_{\alpha}(y)]^2\} \tag{13a}$$

and

$$\tilde{\Pi}_{\alpha}(y)=P\int_{-\infty}^{\infty}\frac{dy_1}{\pi}\frac{\tilde{\Gamma}_{\alpha}(y_1)}{y-y_1}, \tag{13b}$$

where P denotes the principle part integral. Equations (12) and (13) are the equations that will be solved in this section. To obtain the true solutions to the wave-vector–independent "local" linewidth and line-shape functions, one makes the transformations

$$\Gamma_{\alpha}(\omega)=V\tilde{\Gamma}_{\alpha}(\omega/V) \tag{14a}$$

and

$$g_{\alpha}(\omega)=\frac{\tilde{g}_{\alpha}(\omega/V)}{V}. \tag{14b}$$

The first approximation to the wave-vector–dependent dipole linewidth function is,[34] in dimensionless form,

$$\tilde{\Gamma}_{1m}(\vec{q},y)=\frac{2S(S+1)}{3NV^2}\sum_{\vec{q}_1}[J^2(\vec{q}_1)-J(\vec{q}_1)J(\vec{q}-\vec{q}_1)]\tilde{\gamma}_{1m}(y)$$
$$+R[d^{20}_{2,m}(S)]^2\tilde{g}_{2m}(y), \tag{15a}$$

where

$$\tilde{\gamma}_{1m}(y)=\tilde{\Gamma}_{1m}(y)-R[d^{20}_{2,m}(S)]^2\tilde{g}_{2m}(y). \tag{15b}$$

This solution reproduces correctly all of the moments of $\Gamma_{1m}(\vec{q},\omega)$ to order $1/Z$ for all $\vec{q}$. On the other hand, Eqs. (14a) and (14b) reproduce all of the moments of $\Gamma_{lm}(\vec{q},\omega)$ for $l>1$ accurately to order $1/Z$. Thus, the $g_{lm}(\vec{q},\omega)$ for $l>1$ are independent of $\vec{q}$ to that order. The fact that the second term in Eq. (15a) is independent of $\vec{q}$ is a reflection of this fact.

Equations (12) and (13) have been solved numerically by iteration on a computer for all values of S in the range $1\leq S\leq\frac{5}{2}$ and for various values of R in the range $0.0\leq R\leq 5.0$. The results for the "local" dipolar spectral functions $\tilde{g}_{11}(y)$ and $\tilde{g}_{10}(y)$ are summarized in Figs. 4–6. Note that at $R=0.0$, $\tilde{g}_{11}(y)=\tilde{g}_{10}(y)$ and that these functions are independent of S for that value of R. This result is expected from the knowledge that $R=0.0$ implies $D=0.0$ and thus the problem is reduced to that of the isotropic Heisenberg magnet again. Therefore, for $R=0.0$, the solutions for the "local" dipolar functions are the same as those obtained in Ref. 34.

The general behavior of these quantities as functions of R and S is as follows. For constant S, the function $\tilde{g}_{11}(y)$ begins as a fairly narrow Gaussian-like curve for small R. As R increases, the peak height of this function drops and the curve gradually becomes broader and flatter while still retaining its Gaussian-like shape. Finally, at very large R, this function has become virtually a constant over the frequency range for which the $R=0.0$ function is nonzero. This behavior is shown explicitly for $S=1$, $\frac{3}{2}$, 2, and $\frac{5}{2}$ in Fig. 4. For constant S, the function $\tilde{g}_{10}(y)$ also, of course, begins as a Gaussian-like curve at small R. In contrast to $\tilde{g}_{11}(y)$, as R increases, the peak height of $\tilde{g}_{10}(y)$ increases and this function gradually becomes narrower and more sharply peaked. Also, as this narrowing continues, the curve begins to change its shape from Gaussian-like to Lorentzian-like. Finally, at large R, this function has become so narrow and sharply peaked that the $R=0.0$ function is virtually a constant over the frequency range for which the large R function is nonzero. This behavior is shown explicitly for $S=1$, $\frac{3}{2}$, 2, and $\frac{5}{2}$ in Fig. 5. For constant R and varying S the functions $\tilde{g}_{11}(y)$ and $\tilde{g}_{10}(y)$ also have opposite behavior. Starting from a Gaussian-like shape for $S=1$, $\tilde{g}_{11}(y)$ broadens out and becomes flatter on its peak as S is increased, but its Gaussian-like shape is retained. On the other hand, as S is increased, the function $\tilde{g}_{10}(y)$ changes from a Gaussian-like function at $S=1$ to a narrow, sharply peaked, Lorentzian-like function for $S=\frac{5}{2}$. This behavior for $\tilde{g}_{11}(y)$ and $\tilde{g}_{10}(y)$ is shown for $R=0.5$ in Fig. 6.

The term "large R" in the above discussion means the largest value of R for which the computer program could obtain convergent solutions for these functions within a reasonable number of iterations and with the use of a reasonable amount of computer time. A reasonable number of iterations was considered to be of the order of 25 and a reasonable amount of computer time was considered to be of the order of 10–15 min. For most values of S, this "large R" value was $R\sim 5.0$.

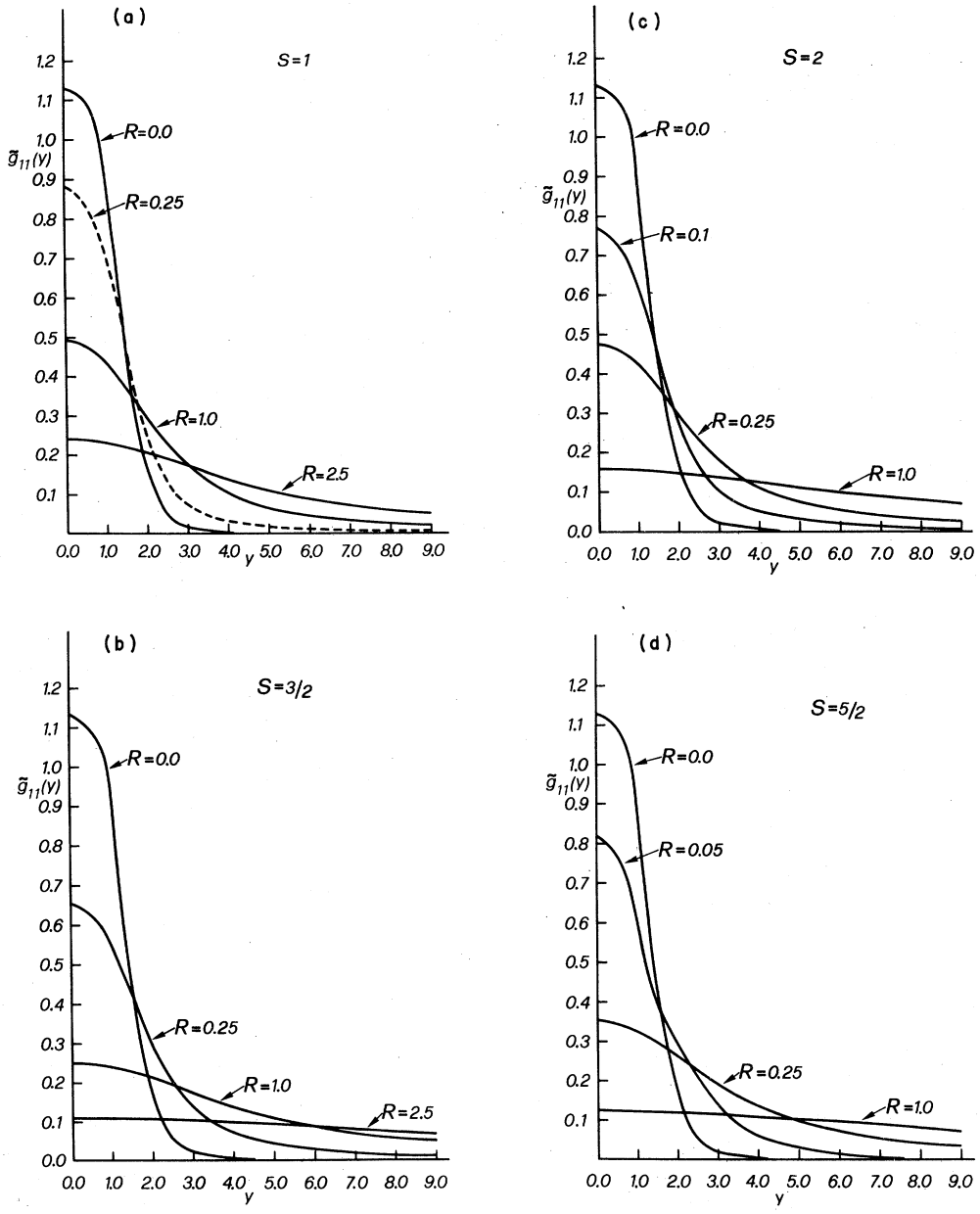

FIG. 4. Dipolar spectral function $\tilde{g}_{11}(y)$ for various S. (a) $S=1$; (b) $S=\frac{3}{2}$; (c) $S=2$; (d) $S=\frac{5}{2}$.

It should be stated at this point that one of the new facts that the above results show is that even with the fairly large spin value of $S=\frac{5}{2}$, one has not yet, even for practical purposes, reached the classical ($S=\infty$) limit where, for a given value of R, the functions $\tilde{g}_{11}(y)$ and $\tilde{g}_{10}(y)$ would no longer vary as a function of S. (In other words, if the classical limit were reached, these functions would have reached saturated values as a function of S.) In fact, for the largest value of R for which solutions were computed, $R=5.0$, the difference between the $\tilde{g}_{11}(y)$ for $S=2$ and that for $S=\frac{5}{2}$ is of the order of 30% for the entire frequency range. Thus, the fact that the spins are quantized is still important, even for $S=\frac{5}{2}$. Similar results hold for $\tilde{g}_{10}(y)$. Also, as R decreases this difference increases. This last point indicates that the classical limit might be approached faster for large values of R than for small values of R. Thus, the size of the uniaxial anisotropy energy to exchange energy ratio appears to have a marked effect on the value of S for which the classical limit is

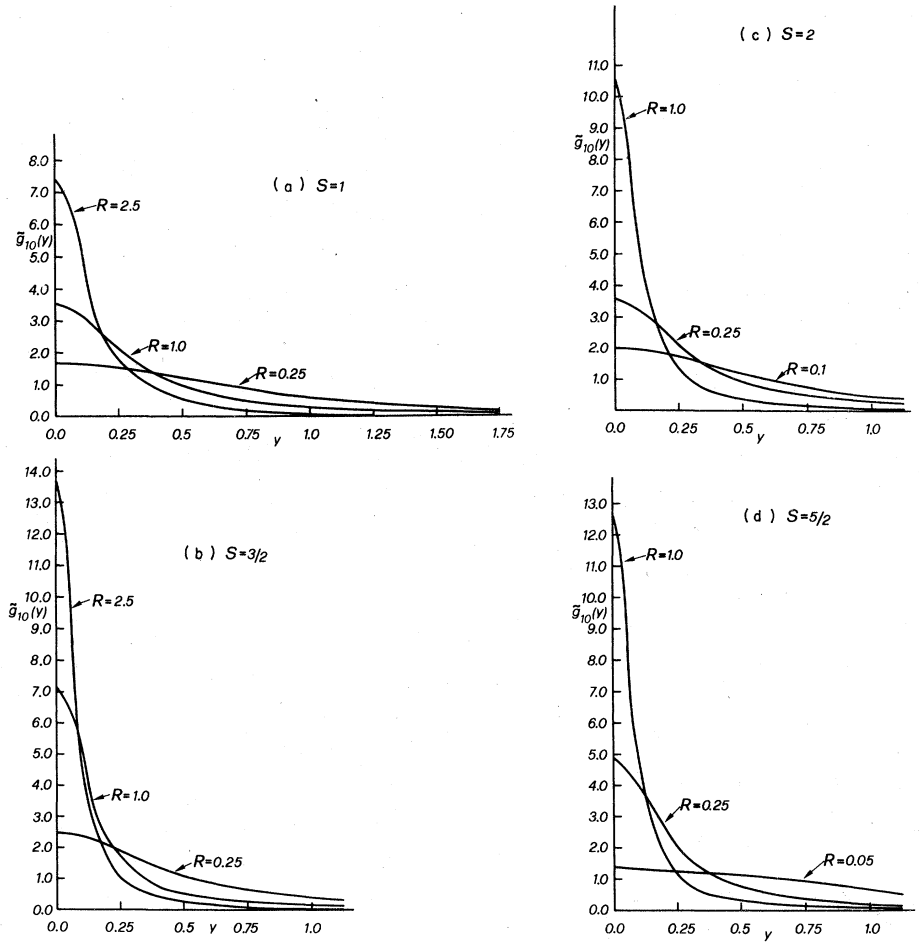

FIG. 5. Same as Fig. 4 but for $\tilde{g}_{10}(y)$.

reached.

In the above context, "classical limit" means the classical limit for all practical purposes. If that limit were reached in this sense the solutions to Eqs. (12) and (13) would no longer depend on S. The true classical limit must, of course, be taken by properly taking the $S=\infty$ limit of Eqs. (12). It is not yet clear exactly how to do this.

Even though the functions $\tilde{g}_{1m}(y)$ are the functions of primary interest, the numerical solutions to Eqs. (12) and (13), of course, yield self-consistently all of the functions $\tilde{g}_{lm}(y)$ for $1 \leq l \leq 2S$. Since, for example, for $S=\frac{5}{2}$, one has 20 such functions, there is clearly neither enough space here nor, in fact, sufficient interest in these functions to show all of them and their various dependences on S and R. The quadrupolar functions $\tilde{g}_{2m}(y)$ are, however, observable in acoustic experiments in magnetic insulators[53] and so are of some intrinsic interest in themselves while the $\tilde{g}_{lm}(y)$ for $l>2$ do not appear to be observable. Therefore, some representative results for the $\tilde{g}_{2m}(y)$ are shown in Fig. 7.

The behavior of the $\tilde{g}_{2m}(y)$ as functions of R and S may be summarized as follows. Again, for $R=0.0$, one has the result $\tilde{g}_{20}(y)=\tilde{g}_{21}(y)=\tilde{g}_{22}(y)$ and that these functions are independent of S in that limit. Thus, in this case, the results for these functions are again the same as found in Ref. 34. For constant S the functions $\tilde{g}_{21}(y)$ and $\tilde{g}_{22}(y)$ behave, as a function of R, in a manner similar to $\tilde{g}_{11}(y)$ while $\tilde{g}_{20}(y)$ behaves somewhat like $\tilde{g}_{10}(y)$. In particular, the functions $\tilde{g}_{21}(y)$ and $\tilde{g}_{22}(y)$ begin, for small R, as broad Gaussian-like curves and become broader with a corresponding decrease in peak height as R is increased until, for $R \gtrsim 1.0$, they are virtually constants over the range for which the $R=0.0$ functions are nonzero. This behavior is summarized in Figs. 7(b) and 7(c). On the other hand, the functions $\tilde{g}_{20}(y)$ be-

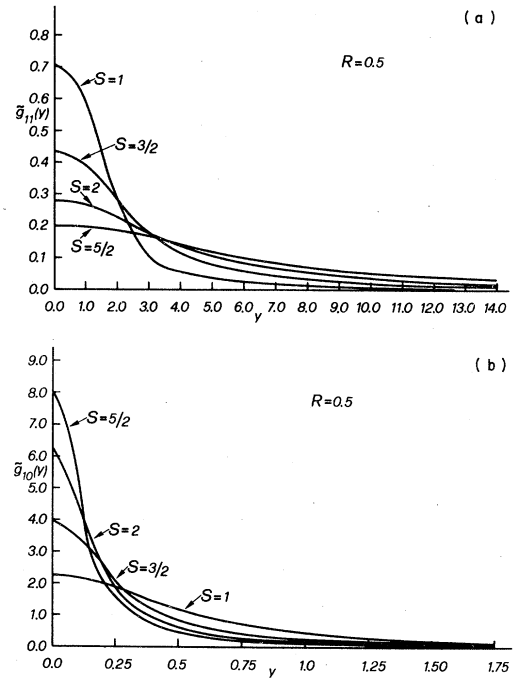

FIG. 6. Dipolar spectral functions for different S at $R=0.5$. (a) $\tilde{g}_{11}(y)$; (b) $\tilde{g}_{10}(y)$.

comes narrower and increases in peak height as R is increased. At the same time, it changes from a Gaussian-like to a Lorentzian-like curve and, for large R, becomes so narrow that the $R=0.0$ function is virtually a constant over the range where the large R function is nonzero. Representative results for this function are shown in Fig. 7(a). For constant R, the functions $\tilde{g}_{2m}(y)$ also behave as a function of S similar to the functions $\tilde{g}_{1m}(y)$ with $\tilde{g}_{21}(y)$ and $\tilde{g}_{22}(y)$, like $\tilde{g}_{11}(y)$, broadening and becoming flatter for increasing S and $\tilde{g}_{20}(y)$, like $\tilde{g}_{10}(y)$, narrowing and becoming more Lorentzian-like for increasing S. In addition, it should be noted that the $\tilde{g}_{2m}(y)$ are in general, for a given R and S, broader functions than the $\tilde{g}_{1m}(y)$ at corresponding R and S.

The general behavior of the $\tilde{g}_{lm}(y)$ for all $l \leq 2S$ can also be described by comparison with the $\tilde{g}_{1m}(y)$. In particular, it was found that, for either constant R and increasing S or constant S and increasing R, the functions $\tilde{g}_{l0}(y)$, like $\tilde{g}_{10}(y)$, narrow and become increasingly Lorentzian-like while the functions $\tilde{g}_{lm}(y)$ for $0<m\leq l$ like $\tilde{g}_{11}(y)$, broaden and become increasingly flat. Also, it is a general fact that for a given R and S, the function $\tilde{g}_{lm}(y)$ is broader and less sharply peaked than the function $\tilde{g}_{l-1,m}(y)$. It is clear that the solutions presented here for the $\tilde{g}_{lm}(y)$ are qualitatively similar to those of JPR. However, since they work in time space and the work here is in frequency space, it is difficult to make a quantitative comparison between the two theories.

It is clear from Eqs. (12) that R is a naturally occuring parameter in those equations. However, in most previous studies of uniaxial anisotropic magnetic systems,[1-8,29,30] the parameter that has been varied is D/J, where J is an exchange constant. To make contact with these previous studies, it is necessary to express the quantity R explicitly in terms of D/J. From the definition of R,

$$R=\frac{D^2}{V^2}=D^2\Big/\frac{2S(S+1)}{3N}\sum_{\vec{q}}[J(\vec{q})]^2. \tag{16}$$

it can be seen that in order to accomplish this it is necessary to assume a form for $J(\vec{q})$ and thus to assume a particular lattice structure.

The main motivation for this work was originally a study of the spin dynamics in substances like NiF_2, CoF_2, FeF_2, and MnF_2. In fact, Sec. V C, the spin-diffusion coefficients and the exchange-narrowed dipolar linewidths will be computed for these substances. Thus, with that application in mind, it is convenient to assume a $J(\vec{q})$ and a lattice structure which are appropriate for those materials. In any case, the dependence of the parameter R on the ratio D/J should not depend too strongly on the choice of lattice structure. All four of the above mentioned compounds possess a rutile structure with first-, second-, and third-neighbor exchange constants.[43-47] In this case, it can be shown that the exchange interaction has the form

$$\begin{aligned}J(\vec{q}) &= 2J_1\cos(q_z c)\\ &\quad + 8J_2\cos(\tfrac{1}{2}q_x a)\cos(\tfrac{1}{2}q_y a)\cos(\tfrac{1}{2}q_z c)\\ &\quad + 2J_3[\cos(q_x a)+\cos(q_y a)].\end{aligned} \tag{17a}$$

where J_1, J_2, J_3 are the first-, second-, and third-neighbor exchange constants, a and c are the lattice constants in the $\hat{a}$ and $\hat{c}$ directions of the rutile structure, and q_x, q_y, q_z are the Cartesian components of the wave vector $\vec{q}$. Using Eq. (17a) in Eq. (16) gives the result

$$R=3D^2/4S(S+1)(J_1^2+4J_2^2+2J_3^2). \tag{17b}$$

Fortunately, for the substances mentioned, it is experimentally found that $J_1, J_3 \ll J_2$.[43-47] Therefore, it will be assumed that the model system described above will have this same property for all values of S and R. In this case, one can neglect J_1^2 and J_3^2 in the denominator of Eq. (17b) and can thus obtain the rather simple expression

$$R=3D^2/16S(S+1)J^2, \tag{17c}$$

where J_2 has been abbreviated as J. Equation (17c) is the form that will be assumed for R for

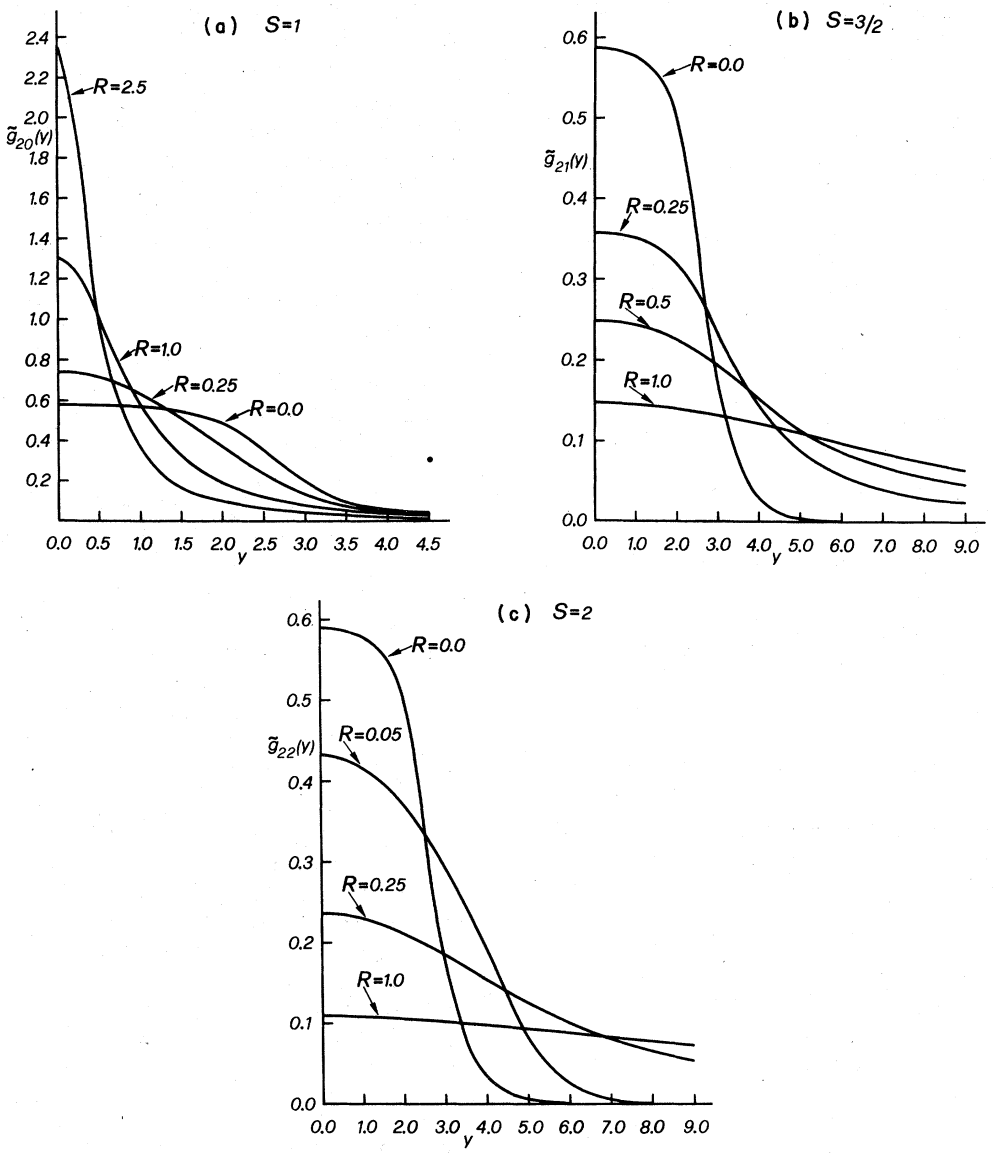

FIG. 7. Representative results for the quadrupolar spectral functions. (a) $\tilde{g}_{20}(y)$, $S=1$; (b) $\tilde{g}_{21}(y)$, $S=\frac{3}{2}$; (c) $\tilde{g}_{22}(y)$, $S=2$.

the rest of the paper. In order to make contact with previous work[1-8, 29, 30] and relate specific values of R to specific values of D/J, for example, the values of R shown in Figs. 4–7, $|D/J|$ given by Eq. (17c) is shown in Table I as a function of R and S.

V. SPIN-DIFFUSION COEFFICIENT AND EXCHANGE-NARROWED DIPOLAR LINEWIDTH

A. Spin-diffusion coefficient

Since, as was discussed in Sec. IV, the spectral functions $g_{lm}(\vec{q}, \omega)$ for $l>1$ are independent of $\vec{q}$ to order $1/Z$ and the "local" solutions $\tilde{g}_{lm}(y)$ are approximations to these functions which are accurate to that order, they are adequate solutions within the accuracy of the theory. On the other hand, the dipolar spectral functions $\tilde{g}_{1m}(\vec{q}, y)$ retain a wave-vector dependence even to order $1/Z$, as can be seen by Eq. (15). The remainder of this paper will be concerned exclusively with these functions. In particular, in this subsection, a discussion will be given as to how one obtains a self-consistent approximation to the $\vec{q}$ dependence of these functions which is accurate to order $1/Z$. Then these approximate $\vec{q}$-dependent solutions will be used to obtain values for the spin-diffusion co-

TABLE I. Table of $|D/J|$ as a function of R and S as given by Eq. (17c).

R \ S	1	$\frac{3}{2}$	2	$\frac{5}{2}$
0.0001	0.0321	0.0447	0.0566	0.0683
0.001	0.1033	0.1414	0.1789	0.2160
0.005	0.2309	0.3162	0.4000	0.4830
0.01	0.3266	0.4472	0.5657	0.6831
0.025	0.5164	0.7071	0.8944	1.0801
0.05	0.7303	1.0000	1.2649	1.5275
0.1	1.0328	1.4142	1.7889	2.1602
0.25	1.6330	2.2361	2.8284	3.14157
0.5	2.3094	3.1623	4.0000	4.8305
0.75	2.8284	3.8730	4.8990	5.9161
1.0	3.2660	4.4721	5.6569	6.8313
2.5	5.1640	7.0711	8.9443	10.8012
5.0	7.3030	10.0000	12.6491	15.2753

efficients as a function of R and S. The treatment given here will be much the same as that given for the isotropic case in Ref. 34.

The starting point to obtain an approximate $\vec{q}$-dependent solution for the $\tilde{g}_{1m}(\vec{q},y)$ is Eq. (15a) which can be rewritten

$$\tilde{\Gamma}^{(1)}_{11}(\vec{q},y)=\alpha(\vec{q})\int_{-\infty}^{\infty}\frac{dy_1}{\pi}\tilde{g}_{10}(y_1)\tilde{g}_{11}(y-y_1) + Rf(S)\tilde{g}_{21}(y), \tag{18a}$$

$$\tilde{\Gamma}^{(1)}_{10}(\vec{q},y)=\alpha(\vec{q})\int_{-\infty}^{\infty}\frac{dy_1}{\pi}\tilde{g}_{11}(y_1)\tilde{g}_{11}(y-y_1), \tag{18b}$$

where

$$\alpha(\vec{q})=\frac{2S(S+1)}{3NV^2}\sum_{\vec{q}_1}[J^2(\vec{q}_1)-J(\vec{q}_1)J(\vec{q}-\vec{q}_1)] \tag{18c}$$

and

$$f(S)=\tfrac{1}{5}[4S(S+1)-3]=\begin{cases}1, & S=1\\ \frac{12}{5}, & S=\frac{3}{2}\\ \frac{21}{5}, & S=2,\\ \frac{32}{5}, & S=\frac{5}{2}.\end{cases} \tag{18d}$$

These equations have been shown explicitly for $m=0$ and $m=1$ in order to try to make the following discussion clearer. The "local" functions $\tilde{g}_{10}(y)$, $\tilde{g}_{11}(y)$, and $\tilde{g}_{21}(y)$ are known self-consistently from the solutions to Eqs. (12). Equations (18) are clearly a first approximation to the $\vec{q}$-dependent linewidth functions $\tilde{\Gamma}_{1m}(\vec{q},y)$, hence the notation $\tilde{\Gamma}^{(1)}_{1m}(\vec{q},y)$ has been used.

A first approximation to the $\vec{q}$-dependent lineshape functions $\tilde{g}_{1m}(\vec{q},y)$ can now be obtained by substituting Eqs. (18) into Eqs. (7) and (8). Before this is done, however, it is convenient to note that the only $\vec{q}$ dependence in Eq. (18) occurs in the quantity $\alpha(\vec{q})$. This is fortunate because it makes the next few steps in the calculation much easier to do numerically. In particular, utilizing this fact enables one to conveniently suppress the $\vec{q}$ dependence of $\alpha(\vec{q})$, and thus that of Eq. (18), and to instead treat that quantity as a parameter α which varies over the physically allowable range for $\alpha(\vec{q})(2.0\geq\alpha\geq 0.0)$. At the end of the calculation the $\vec{q}$ dependence of $\alpha(\vec{q})$ can then be explicitly reinserted to obtain the $\vec{q}$ dependence of the function $\tilde{\Gamma}_{1m}(\vec{q},y)$ or $\tilde{g}_{1m}(\vec{q},y)$. This scheme results in a considerable savings in both the complexity of the numerical analysis and the amount of computer time required to do the calculation because, with it, one has only a one-dimensional parameter α to keep track of rather than a three-dimensional wave vector $\vec{q}$.

With this convention, the substitution of Eqs. (18) into Eqs. (7) and (8) yields

$$\tilde{g}^{(1)}_{1m}(\alpha,y)=\tilde{\Gamma}^{(1)}_{1m}(\alpha,y)/\{[y-\tilde{\Pi}^{(1)}_{1m}(\alpha,y)]^2+[\tilde{\Gamma}^{(1)}_{1m}(\alpha,y)]^2\} \tag{19a}$$

and

$$\tilde{\Pi}^{(1)}_{1m}(\alpha,y)=P\int_{-\infty}^{\infty}\frac{dy_1}{\pi}\frac{\tilde{\Gamma}^{(1)}_{1m}(\alpha,y_1)}{y-y_1}, \tag{19b}$$

where $\tilde{\Gamma}^{(1)}_{1m}(\alpha,y)$ signifies the $\tilde{\Gamma}_{1m}(\vec{q},y)$ of Eqs. (18), with $\alpha=\alpha(\vec{q})$ treated as a parameter, and the superscripts again denote the first approximation. The specific $\vec{q}$ dependence of $\tilde{g}^{(1)}_{1m}(\vec{q},y)$ can be obtained by assuming a form for the exchange interaction $J(\vec{q})$, calculating the $\vec{q}$ dependence of $\alpha(\vec{q})$ from Eq. (18c) and substituting that result into Eqs. (18a), (18b) and (19).

Although the above scheme yields a first approximation for the $\tilde{g}_{1m}(\vec{q},y)$, a better approximation can be obtained from this result by one more "iteration" through Eqs. (7), (8), and (9a). In other words, the next approximations to the $\Gamma_{1m}(\vec{q},y)$ can be obtained from the $\tilde{g}^{(1)}_{1m}(\vec{q},y)$ by substitution of those functions into the right-hand side of Eq. (9a). When this is done, the result is

$$\tilde{\Gamma}^{(2)}_{11}(\vec{q},y)=\frac{2S(S+1)}{3NV^2}\sum_{\vec{q}_1}[J^2(\vec{q}_1)-J(\vec{q}-\vec{q}_1)J(\vec{q}_1)] \times\Delta_{11}(\alpha(\vec{q}),y)+Rf(S)\tilde{g}_{21}(y), \tag{20a}$$

$$\tilde{\Gamma}^{(2)}_{10}(\vec{q},y)=\frac{2S(S+1)}{3NV^2}\sum_{\vec{q}_1}[J^2(\vec{q}_1)-J(\vec{q}-\vec{q}_1)J(\vec{q}_1)] \times\Delta_{10}(\alpha(\vec{q}),y), \tag{20b}$$

where

$$\Delta_{11}(\alpha,y)=\int_{-\infty}^{\infty}\frac{dy_1}{\pi}\tilde{g}^{(1)}_{10}(\alpha,y_1)\tilde{g}^{(1)}_{11}(\alpha,y-y_1) \tag{20c}$$

and

TABLE II. Coefficients in Eqs. (21) for $S=1$.

R	a_{-2}	a_{-1}	a_0	a_1	a_2	b_{-1}	b_0	b_1	b_2
0.0	0.0	0.5689	0.2760	0.0318	0.0022	0.5689	0.2760	0.0318	0.0022
0.25	0.0	0.1874	1.547	−1.393	0.4032	0.1267	1.169	−0.9643	0.2698
0.50	0.0	0.1320	1.330	−1.155	0.3213	0.0697	0.9566	−0.8035	0.2197
0.75	0.0	0.1318	0.9739	−0.7750	0.2044	0.0507	0.7876	−0.6763	0.1849
1.00	0.0	0.1476	0.6443	−0.4322	0.1015	0.0428	0.6602	−0.5784	0.1590
2.50	0.0	0.1918	0.3138	−0.2842	0.0675	0.0326	0.3069	−0.2861	0.0813
5.00	0.0171	0.0741	0.0301	−0.0032	0.0	0.0212	0.1398	−0.1286	0.0315

$$\Delta_{10}(\alpha,y)=\int_{-\infty}^{\infty}\frac{dy_1}{\pi}\tilde{g}_{11}^{(1)}(\alpha,y_1)\tilde{g}_{11}^{(1)}(\alpha,y-y_1). \qquad (20d)$$

In Eqs. (20a) and (20b) α has been shown as a function of $\vec{q}$ to emphasize the fact that it must be treated as such in order to explicitly evaluate the $\tilde{\Gamma}_{1m}^{(2)}(\vec{q},y)$. On the other hand, the functions $\Delta_{1m}(\alpha,y)$ in Eqs. (20c) and (20d) can be evaluated with α treated as a parameter. In the latter two equations, it has been assumed that since the main quantities of interest are to be evaluated near $\vec{q}=0$ and since Eqs. (20) are only expected to be accurate to order $1/Z$, one can replace $\tilde{g}_{1m}(\vec{q}_1,y_1)\tilde{g}_{1m}(\vec{q}-\vec{q}_1,y-y_1)$ by $\tilde{g}_{1m}(\vec{q}_1,y_1)\tilde{g}_{1m}(\vec{q}_1,y-y_1)$ in Eq. (9a). In the $\vec{q}\to 0$ limit, such a replacement should make errors smaller than $1/Z$. Finally, the lack of a $\vec{q}$ dependence of $\tilde{g}_{21}(\vec{q},y)$ to order $1/Z$ is seen explicitly in Eq. (20a).

Equations (20) are good second approximation to the linewidth functions $\tilde{\Gamma}_{1m}(\vec{q},y)$ which should be accurate to order $1/Z$. A further approximation to $\tilde{g}_{1m}(\vec{q},y)$ could now be obtained, if one desired, by the substitution of Eqs. (20) into Eqs. (7) and (8). However, this will not be done here, because the spin-diffusion coefficients can be calculated from the $\tilde{\Gamma}_{1m}^{(2)}(\vec{q},y)$.

The functions $\tilde{\Gamma}_{1m}^{(1)}(\alpha,y)$, $\tilde{\Pi}_{1m}^{(1)}(\alpha,y)$, $\tilde{g}_{1m}^{(1)}(\alpha,y)$, and $\Delta_{1m}(\alpha,y)$ have been evaluated numerically for various values of α in the range $0.0\leq\alpha\leq 2.0$ and for various y. The explicit $\vec{q}$ dependence of the $\Delta_{1m}(\alpha,y)$ which is necessary for the evaluation of Eqs. (20a) and (20b) can be found for a given y by first fitting the numerical results for $\Delta_{1m}(\alpha,y)$ to a polynomial in α and then by substituting the functional form for $\alpha(\vec{q})$ into the polynomial. Once this polynomial and the functional form of $\alpha(\vec{q})$ are specified, the $\vec{q}_1$ sum in Eqs. (20a) and (20b) can be done and an approximation for $\tilde{\Gamma}_{1m}^{(2)}(\vec{q},y)$ can be found. Since, for the calculation of the spin-diffusion coefficient, only the $y=0$ limit of Eqs. (20) is of interest, only that limit will be discussed here. When fit to polynomials in α, the functions $\Delta_{1m}(\alpha,0)$ take the forms

$$\Delta_{11}(\alpha,0)=a_{-2}/\alpha^2+a_{-1}/\alpha+a_0+a_1\alpha+a_2\alpha^2 \qquad (21a)$$

and

$$\Delta_{10}(\alpha,0)=b_{-1}/\alpha+b_0+b_1\alpha+b_2\alpha^2, \qquad (21b)$$

where the a_i and b_i are of course, functions of R and S. Typical values of these quantities for $1\leq S\leq\frac{5}{2}$ and various R are shown in Tables II–V. For the coefficients used in the following calculations, the forms (21a) and (21b) fit the computer generated functions to within 0.5% for all values of α.

In the following calculation, the exchange interaction $J(\vec{q})$ will be assumed to be of the form [Eq. (17a)] relevant for the rutile lattice structure with lattice parameters a and c. Also, it will again be assumed, following experimental evidence in rutile paramagnetic compounds, that $J_1, J_3 \ll J_2$.[43-47] Under these conditions, $\alpha(\vec{q})$ is given by

$$\alpha(\vec{q})=1-\cos(\tfrac{1}{2}q_xa)\cos(\tfrac{1}{2}q_ya)\cos(\tfrac{1}{2}q_zc). \qquad (22)$$

If Eqs. (22), (21), and (20) (evaluated at $y=0$) are now combined and the wave-vector sums in Eqs.

TABLE III. Coefficients in Eqs. (21) for $S=\frac{3}{2}$.

R	a_{-2}	a_{-1}	a_0	a_1	a_2	b_{-1}	b_0	b_1	b_2
0.0	0.0	0.5689	0.2760	0.0318	0.0022	0.5689	0.2760	0.0318	0.0022
0.25	0.0	0.1542	1.154	−0.9947	0.2745	0.0754	0.8865	−0.7426	0.2052
0.50	0.0	0.2122	0.3013	−0.1098	0.0095	0.0564	0.5558	−0.5072	0.1422
0.75	0.0089	0.1399	0.2267	−0.0666	0.0	0.0510	0.3857	−0.3613	0.1027
1.00	0.0145	0.1029	0.1753	−0.0504	0.0	0.0475	0.2839	−0.2686	0.0771
2.50	0.0239	0.0544	0.0293	−0.0030	0.0	0.0335	0.0940	−0.0821	0.0242
5.00	0.0248	0.0430	0.0078	0.0030	0.0	0.0280	0.0609	−0.0449	0.0114

TABLE IV. Coefficients in Eqs. (21) for $S=2$.

R	a_{-2}	a_{-1}	a_0	a_1	a_2	b_{-1}	b_0	b_1	b_2
0.0	0.0	0.5689	0.2760	0.0318	0.0022	0.5689	0.2760	0.0318	0.0022
0.25	0.0	0.2025	0.4825	−0.3047	0.0681	0.0638	0.6085	−0.5452	0.1530
0.50	0.0126	0.1194	0.1990	−0.0583	0.0	0.0532	0.3021	−0.2996	0.0860
0.75	0.0190	0.0790	0.1270	−0.0347	0.0	0.0467	0.2010	−0.1867	0.0545
1.00	0.0216	0.0637	0.0838	−0.0204	0.0	0.0420	0.1453	−0.1312	0.0386
2.50	0.0254	0.0438	0.0144	0.0012	0.0	0.0302	0.0660	−0.0515	0.0140
5.00	0.0245	0.0428	0.0055	0.0035	0.0	0.0272	0.0593	−0.0427	0.0105

(20a) and (20b) are done, one finally obtains an approximation to the $\vec{q}$ dependence of $\tilde{\Gamma}_{1m}(\vec{q},0)$. In the small-$\vec{q}$ limit ($|\vec{q}|a, |\vec{q}|c \ll 1$) the result is

$$\tilde{\Gamma}^{(2)}_{11}(\vec{q},0) \simeq |\vec{q}|^2\tilde{D}_1 + Rf(S)\tilde{g}_{21}(0), \tag{23a}$$

$$\tilde{\Gamma}^{(2)}_{10}(\vec{q},0) \simeq |\vec{q}|^2\tilde{D}_0, \tag{23b}$$

where

$$\tilde{D}_1 = (a^2\sin^2\theta + c^2\cos^2\theta)B_1(R,S) \tag{23c}$$

and

$$\tilde{D}_0 = (a^2\sin^2\theta + c^2\cos^2\theta)B_0(R,S). \tag{23d}$$

The quantities $\tilde{D}_1, \tilde{D}_0$ are, by definition,[33,54] the dimensionless spin-diffusion coefficients belonging to the spectral functions $\tilde{g}_{11}(\vec{q},y)$ and $\tilde{g}_{10}(\vec{q},y)$, respectively. By Eq. (14a), in order to obtain the physically observable diffusion coefficients, one must multiply these dimensionless quantities by V which is given under these conditions by $V = 4[\frac{1}{3}S(S+1)]^{1/2}J_2$. In Eqs. (23c) and (23d), θ is the angle that the wave vector $\vec{q}$ makes with the c axis of the crystal and the R- and S-dependent parts of $\tilde{D}_1$ and $\tilde{D}_0$ are given explicitly by

$$B_1(R,S) = 0.6501a_{-2} + 0.2176a_{-1} + 0.1250a_0 + 0.0868a_1 + 0.0661a_2 \tag{24a}$$

and

$$B_0(R,S) = 0.2176b_{-1} + 0.1250b_0 + 0.0868b_1 + 0.0661b_2. \tag{24b}$$

These functions have been evaluated for various R and for $1 \leq S \leq \frac{5}{2}$ and the results are summarized in Figs. (8a) and (8b). From these figures it can be seen that, for a given S, both spin-diffusion coefficients fall off rather quickly with increasing R at small R and finally reach a virtually constant value for R between 2.0 and 5.0. Thus there is a "saturation point" where they will no longer depend on R. Also, these figures show that for a given $R>0$, as S is increased the diffusion coefficients decrease but this decrease becomes less the larger the value of S. This is an indication that the classical limit, where $\tilde{D}_1$ and $\tilde{D}_0$ would no longer depend on S, is being rapidly approached even for $S=\frac{5}{2}$. This should be contrasted with the remarks made in Sec. IV where it was noted that for a given R, the classical limit with respect to the $\tilde{g}_{1m}(y)$ had not been reached even for $S=\frac{5}{2}$. From these two results, it can be concluded that the rapidity of the approach to the classical limit, in the sense referred to here, depends on just what physical quantity one is referring to. Thus for a given R, this limit is being approached faster with respect to the $\tilde{D}_1$ and $\tilde{D}_0$ than with respect to the spectral functions. Furthermore, as was the case with the $\tilde{g}_{1m}(y)$, this limit is approached faster for some values of R than others. In this case, the largest discrepancy between the values of the spin-diffusion coefficients at one value of S and their values at the next higher value of S occurs for $0.25 \leq R \leq 1.25$.

It should be noted that the magnitudes of $\tilde{D}_1$ and $\tilde{D}_0$ depend on the lattice constants a and c as well as the angle θ that $\vec{q}$ makes with the c axis. Fur-

TABLE V. Coefficients in Eqs. (21) for $S=\frac{5}{2}$.

R	a_{-2}	a_{-1}	a_0	a_1	a_2	b_{-1}	b_0	b_1	b_2
0.0	0.0	0.5689	0.2760	0.0318	0.0022	0.5689	0.2760	0.0318	0.0022
0.25	0.0065	0.1679	0.2324	−0.0683	0.0	0.0588	0.4204	−0.3854	0.1100
0.50	0.0178	0.0798	0.1377	−0.0386	0.0	0.0480	0.2085	−0.1871	0.0550
0.75	0.0193	0.0640	0.1006	−0.0265	0.0	0.0425	0.1575	−0.1325	0.0379
1.00	0.0231	0.0523	0.0514	−0.0101	0.0	0.0370	0.1043	−0.0871	0.0248
2.50	0.0224	0.0474	0.0357	−0.0052	0.0	0.0329	0.0894	−0.0683	0.0180
5.00	0.0221	0.0509	0.0418	−0.0073	0.0	0.0339	0.0973	−0.0790	0.0218

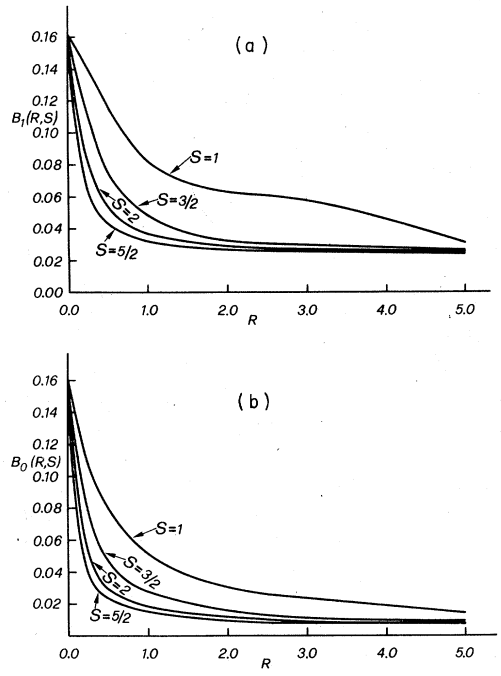

FIG. 8. R- and S-dependent parts of the spin-diffusion coefficients. (a) $B_1(R,S)$; (b) $B_0(R,S)$.

thermore, since there is a $\vec{q}$-independent part to $\tilde{\Gamma}_{11}^{(2)}(\vec{q},0)$, the $\vec{q}$-dependent part and thus $\tilde{D}_1$ could conceivably be masked from experimental observation for some values of R, S, and $|\vec{q}|$. One can obtain some idea where this effect might occur by examining Eq. (23a) in detail. Using that equation along with Eq. (23c) at $\theta=\frac{1}{2}\pi$, a reasonable criterion for the observation of $\tilde{D}_1$ can be seen to be

$$|\vec{q}|^2a^2 > Rf(S)\tilde{g}_{21}(0)/B_1(R,S) \equiv Q. \tag{25}$$

The ratio Q, in Eq. (25) has been plotted in Fig. 9 as a function of R for $1 \leq S \leq \frac{5}{2}$. In order to have Eq. (25) and the criterion for the validity of Eq. (23a) ($|\vec{q}|^2a^2 < 1$) satisfied at the same time, it is obvious that the relationship $Q < 1$ must hold. From Fig. 9, it can be seen that this relationship occurs only for small R. From that figure, the criteria for the observability of $\tilde{D}_1$ are the following: for $S=1$, $R<0.268\,75$; for $S=\frac{3}{2}$, $R<013\,125$; for $S=2$, $R<0.075$; and for $S=\frac{5}{2}$, $R<0.05$. For all values of R greater than these critical values spin diffusion is effectively quenched or masked for the spectral function $\tilde{g}_{11}(\vec{q},y)$. Fortunately, most compounds found in nature satisfy the above criteria. Finally, it should be noted that, contrary to what one would naively expect, $\tilde{D}_1(R=0)=\tilde{D}_0(R=0)$ is not exactly equal to the results for the dimensionless diffusion coefficient obtained in Ref. 34. This is because the lattice used in that reference had the simple cubic structure, rather than the rutile structure used here.

B. Exchange-narrowed dipolar linewidth

The exchange-narrowed dipolar linewidths of paramagnetic systems have been of considerable theoretical interest for many years.[9,55-57] but have been approached from the microscopic viewpoint only in the last few years.[34,38] It is possible to calculate such linewidths as functions of R and S by the use of the above self-consistent results for $\Delta_{11}(\alpha,0)$ and $\Delta_{10}(\alpha,0)$ along with the introduction of one other auxiliary function that can be calculated from the self-consistent functions discussed in Sec. IV.

If, in addition to the interaction of Eq. (1), the Hamiltonian contains dipole-dipole interactions, an extra term will be added to that equation which has the form

$$H' = \tfrac{1}{2}\sum_{i,j;a,b} I_{ab}(i,j)S_a(i)S_b(j), \tag{26a}$$

where

$$I_{ab}(i,j) \equiv I_{ab}(\vec{r}) = (\gamma_e\hbar)^2[\delta_{ab} - 3(r_a r_b/r^2)]/r^3. \tag{26b}$$

Here $\vec{r} \equiv \vec{r}_i - \vec{r}_j$, and γ_e is the electron gyromagnetic ratio. With this additional interaction, the derivation of the formalism for the correlation functions will carry through exactly as in Sec. III for anisotropic exchange if one makes the replacement

$$J_{ab} \to J_{ab} + I_{ab} \tag{27}$$

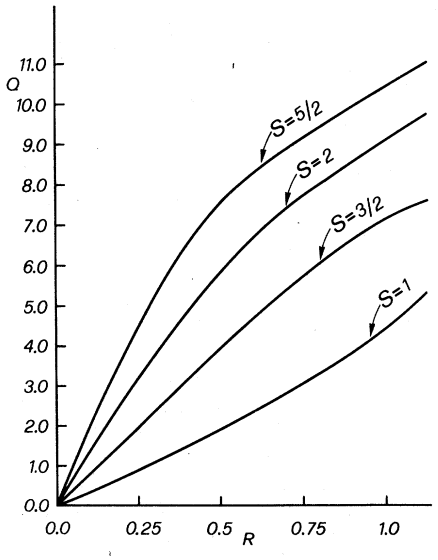

FIG. 9. Ratio Q defined Eq. (25) as a function R and S.

throughout the derivation. Thus, Eq. (6a) for the dipole self-energy functions retains the same functional form even in the presence of the dipolar interaction. It will be assumed in the following discussion that the replacement, Eq. (27), has been made. Note, now, that for systems of practical interest, $J_{ab} \gg I_{ab}$. Thus, it is reasonable to treat the effect of the dipolar interaction on the correlation functions as a small perturbation on the self-consistent solutions obtained in the absence of a dipolar interaction. The effect of the dipolar interaction on the linewidth, which is the effect of interest here, can thus be obtained by the following scheme.

If, after making the replacement, Eq. (27), one takes the imaginary part of Eq. (6a) and Fourier transforms the result, one has the linewidth function of interest $\Gamma_{1m}(\vec{q},\omega)$. The next step is to pass to the isotropic exchange limit, as in Sec. IV, but still retaining a finite dipolar interaction. Note that at $\vec{q}=0$, the part of the resulting $\Gamma_{1m}(\vec{q},\omega)$ which depends explicitly on the isotropic exchange interaction will vanish. [See, for example, Eq. (9a).] Thus, since $J(\vec{q}) \gg I_{ab}(\vec{q})$ the only part of the Brillouin zone where the dipolar interaction will make an important contribution to the functions $\Gamma_{1m}(\vec{q},\omega)$ is near $\vec{q}=0$. In other words, it is reasonable, for $\vec{q}\neq 0$, to neglect the dependence of the $\Gamma_{1m}(\vec{q},\omega)$ on the $I_{ab}(\vec{q})$. Therefore, by Eq. (8), the dependence of the $g_{1m}(\vec{q},\omega)$ on $I_{ab}(\vec{q})$ for $\vec{q}\neq 0$ can also be neglected to a good approximation. Thus, the dipolar interaction has virtually no effect, for $\vec{q}\neq 0$, on the self-consistent solutions for $\Gamma_{1m}(\vec{q},\omega)$ and $g_{1m}(\vec{q},\omega)$ obtained earlier in this paper and will only affect those functions near $\vec{q}=0$. The error made in not taking the dipolar interaction into account self-consistently is discussed at the end of this subsection.

It is now straightforward to find the effects of the dipolar interaction at $\vec{q}=0$. Returning to the $\Gamma_{1m}(\vec{q},\omega)$ obtained by the method in the preceding paragraph, one sees that the $\vec{q}=0$ limit of that function depends, because the explicit dependence on $J(\vec{q})$ will vanish in that limit, on a sum over the Brillouin zone in which the summand consists of the square of the Fourier-transformed dipolar energy $I_{ab}(\vec{q})$ multiplied by the frequency convolution of two wave-vector and frequency-dependent dipolar spectral functions $g_{1m}(\vec{q},\omega)$. By the discussion in the preceding paragraph, these spectral functions can, except in a very small part of the Brillouin zone, be approximated to a high degree of accuracy by the self-consistent solutions to the isotropic exchange case obtained earlier. It will be assumed here that it is sufficient to approximate the dimensionless versions of these functions by the functions $\tilde{g}^{(1)}_{1m}(\alpha,y)$ which were discussed in Sec. V A. When this approximation is made and the $\omega=0$ limit of the resulting equation is also taken, the dimensionless linewidths take the form

$$\tilde{\Gamma}^D_1 \equiv \tilde{\Gamma}_{11}(\vec{q}=0,\omega=0) = \frac{S(S+1)}{3V^2N}\sum_{\vec{q}}\{\{[I_{zz}(\vec{q}) - \tfrac{1}{2}I_{xx}(\vec{q}) - \tfrac{1}{2}I_{yy}(\vec{q})]^2 + \tfrac{1}{4}[I_{xx}(\vec{q}) - I_{yy}(\vec{q})]^2 + [I_{xy}(\vec{q})]^2\}\Delta_{11}(\alpha(\vec{q}),0)$$
$$+ \{[I_{xz}(\vec{q})]^2 + [I_{yz}(\vec{q})]^2\}[\tfrac{3}{2}\Delta_{10}(\alpha(\vec{q}),0) + \Delta_{00}(\alpha(\vec{q}),0)]\} + Rf(S)\tilde{g}_{21}(0) \qquad (28a)$$

and

$$\tilde{\Gamma}^D_0 \equiv \tilde{\Gamma}_{10}(\vec{q}=0,\omega=0) = \frac{S(S+1)}{3V^2N}\sum_{\vec{q}}[\{[I_{xx}(\vec{q}) - I_{yy}(\vec{q})]^2 + 4[I_{xy}(\vec{q})]^2\}\Delta_{11}(\alpha(\vec{q}),0) + \{[I_{xz}(\vec{q})]^2 + [I_{yz}(\vec{q})]^2\}\Delta_{10}(\alpha(\vec{q}),0)], \qquad (28b)$$

where $\Delta_{11}(\alpha,y)$ and $\Delta_{10}(\alpha,y)$ are defined in Eqs. (20c) and (20d), $\alpha(\vec{q})$ is defined in Eq. (18c), and $\Delta_{00}(\alpha,y)$ is defined by

$$\Delta_{00}(\alpha,y) = \int_{-\infty}^{\infty}\frac{dy_1}{\pi}\tilde{g}^{(1)}_{10}(\alpha,y_1)\tilde{g}^{(1)}_{10}(\alpha,y-y_1). \qquad (28c)$$

The $\omega=0$ limit has been taken in Eqs. (28) because the dipolar linewidths are only appreciable in that limit. Equations (28) reduce, of course, to Eq. (42) of Ref. 34 in the $R=0.0$ (zero uniaxial anisotropy) limit.

The task of calculating the two dipolar linewidths $\tilde{\Gamma}^D_1$ and $\tilde{\Gamma}^D_0$ has now been reduced to that of evaluating the wave-vector sums which occur in Eqs. (28). To accomplish this, as was done with $\Delta_{11}(\alpha,0)$ and $\Delta_{10}(\alpha,0)$, the function $\Delta_{00}(\alpha,y)$ was generated numerically as a function of α and the results were fit to a polynomial of the form

$$\Delta_{00}(\alpha,0) = c_{-2}/\alpha_2 + c_{-1}/\alpha + c_0 + c_1\alpha + c_2\alpha^2, \qquad (29)$$

where the c_i are, of course, functions of R and S. Some typical c_i are listed in Tables VI and VII. The wave-vector sums in Eqs. (28) have been carried out for various R and for $1 \leq S \leq \frac{5}{2}$. Since dipolar forces are long ranged, it is necessary to include the forces of several neighbor shells in the wave-vector sums in Eqs. (28). Therefore, in evaluating these sums, the first- through fifth-neighbor shells of the rutile structure were in-

TABLE VI. Coefficients in Eq. (29) for $S=1$ and $S=\frac{3}{2}$.

	$S=1$					$S=\frac{3}{2}$				
R	c_{-2}	c_{-1}	c_0	c_1	c_2	c_{-2}	c_{-1}	c_0	c_1	c_2
0.0	0.0	0.5689	0.2760	0.0318	0.0022	0.0	0.5689	0.2760	0.0318	0.0022
0.25	0.0	0.2343	1.934	−1.741	0.5040	0.0	0.1928	1.443	−1.243	0.3431
0.50	0.0	0.1650	1.663	−1.444	0.4016	0.0	0.2653	0.3766	−0.1313	0.0119
0.75	0.0	0.1648	1.217	−0.9688	0.2555	0.0134	0.1749	0.2834	−0.0833	0.0
1.00	0.0	0.1845	0.8054	−0.5403	0.1269	0.0218	0.1286	0.2191	−0.0630	0.0
2.50	0.0	0.2400	0.3923	−0.3553	0.0844	0.0359	0.0680	0.0366	−0.0038	0.0
5.00	0.0251	0.0926	0.0376	−0.0040	0.0	0.0372	0.0538	0.0098	0.0038	0.0

cluded. At that point, the differences in the linewidths at a given R and S for each succeeding approximation were of the order of (1–2)% as is illustrated for $\tilde{\Gamma}_0^D$ in Table VIII for the particular case of $R=0.25$ and $S=1$. Thus it was thought that little could be gained by including more neighbors since the expected accuracy of the theory is only $1/Z$, where Z is the number of *second* neighbors (because only second neighbor exchange is kept) and is equal to 8 for the rutile structure. In Table VIII and in the following linewidth calculations, only second-neighbor *exchange* forces are assumed and J denotes J_2.

When the wave-vector sums in Eqs. (28) are carried out as described above the results have the form

$$\tilde{\Gamma}_1^D=(\hbar^4\gamma_e^4/a^6J^2)E_1(R,S)+Rf(S)\tilde{g}_{21}(0) \qquad (30a)$$

and

$$\tilde{\Gamma}_0^D=(\hbar^4\gamma_e^4/a^6J^2)E_0(R,S), \qquad (30b)$$

where $E_1(r,S)$ and $E_0(R,S)$ are plotted as a function of R for $1\leq S\leq\frac{5}{2}$ in Figs. 10(a) and 10(b). These functions were obtained under the assumption, approximately valid for the rutile compounds of interest, that the ratio c/a of the lattice constants is $\frac{2}{3}$. If an infinite number of neighbor shells had been included in the dipolar sum, one would have had $\tilde{\Gamma}_0^D|_{R=0}=\tilde{\Gamma}_1^D|_{R=0}$. From Figs. 10(a) and 10(b), however, it can be seen that such is not the case with the inclusion of only five neighbor shells since the calculations of $\tilde{\Gamma}_0^D$ and $\tilde{\Gamma}_1^D$ require the summation to be done with the inclusion of different dipolar functions $I_{ab}(\vec{q})$ of the rutile lattice. It should be noted, however, that the difference between the two linewidths at $R=0.0$ is much less than the expected $1/Z$ inaccuracy of the theory. Furthermore neither $\tilde{\Gamma}_0^D|_{R=0}$ nor $\tilde{\Gamma}_1^D|_{R=0}$ are equal to the result obtained in Ref. 28 since, in that reference, the dipolar sums were done over the simple cubic, rather than rutile, lattice.

As can be seen from Figs. 10(a) and 10(b) the functions $E_1(R,S)$ and $E_0(R,S)$ behave similarly to the functions $B_1(R,S)$ and $B_0(R,S)$ associated with the diffusion coefficients. In particular, for a given S they fall off rapidly with increasing R, soon reaching a saturated value. Also, as a function of S for constant R they are rapidly approaching the classical limit where the dipolar linewidths will be independent of S. Thus the dipolar linewidths appear, like the diffusion coefficients, to be approaching the classical limit faster than the functions $\tilde{g}_{lm}(y)$ themselves.

The second term in Eq. (30a) is going to be large for almost all R and S. In particular, it will in general be much larger than the first term in that equation. Thus, the first term in the linewidth $\tilde{\Gamma}_1^D$ is probably unobservable for any R and S and exchange narrowing is effectively quenched by the anisotropy for the spectral function $\tilde{g}_{11}(\vec{q},y)$.

By not taking into account the dipolar interaction self-consistently, an error of the order of $\tilde{\Gamma}_0^D/$

TABLE VII. Coefficients in Eq. (29) for $S=2$ and $S=\frac{5}{2}$.

	$S=2$					$S=\frac{5}{2}$				
R	c_{-2}	c_{-1}	c_0	c_1	c_2	c_{-2}	c_{-1}	c_0	c_1	c_2
0.0	0.0	0.5689	0.2760	0.0318	0.0022	0.0	0.5689	0.2760	0.0318	0.0022
0.25	0.0	0.2531	0.6031	−0.3809	0.0851	0.0098	0.2099	0.2905	−0.0854	0.0
0.5	0.0189	0.1493	0.2488	−0.0729	0.0	0.0267	0.0998	0.1721	−0.0483	0.0
0.75	0.0285	0.0988	0.1588	−0.0434	0.0	0.0290	0.0800	0.1258	−0.0331	0.0
1.00	0.0324	0.0796	0.1048	−0.0255	0.0	0.0347	0.0654	0.0643	−0.0126	0.0
2.50	0.0381	0.0548	0.0180	0.0015	0.0	0.0336	0.0594	0.0446	−0.0065	0.0
5.00	0.368	0.0535	0.0069	0.0044	0.0	0.0332	0.0636	0.0523	−0.0091	0.0

TABLE VIII. Exchange-narrowed dipolar linewidth Γ_0^D for $R=0.25$ and $S=1$ for each succeeding neighbor shell.

Number of shells included	$\frac{J^2\Gamma_0^D a^6}{\hbar^4\gamma_e^4}$
2	12.0094
3	18.2814
4	20.9365
5	21.2113

$\tilde{D}_0|\vec{q}|^2$ has been made in calculating the spectral function $\tilde{g}_{10}(\vec{q},y)$ and a similar error has been made in calculating the spectral function $\tilde{g}_{11}(\vec{q},y)$. The dipolar interaction will only matter in the calculation of these functions when this ratio is not very small compared to 1. Using reasonable values for the exchange and dipolar energies, for example, those found for rutile compounds in the literature,[43-47] one finds that such a situation will only occur for $|\vec{q}|a<10^{-2}$ or in a volume in $\vec{q}$ space which is only around 10^{-6} of the total volume of the first Brillouin zone. Since all wave vectors in Eqs. (28) are summed over, the dipolar interaction is indeed negligible in the calculation of $\tilde{g}_{11}(\vec{q},y)$ and $\tilde{g}_{10}(\vec{q},y)$.

C. Diffusion coefficients and dipolar linewidths for NiF_2, CoF_2, FeF_2, and MnF_2

Using the exchange, anisotropy, and lattice parameters obtained in Refs. 43–47 and 58, and summarized in Table IX, the spin-diffusion coefficients and dipolar linewidths have been calculated for the compounds $NiF_2(S=1)$, $CoF_2(S=\frac{3}{2})$, $FeF_2(S=2)$, and $MnF_2(S=\frac{5}{2})$. The values of R quoted in Table IX have been computed assuming $J_1, J_3 \ll J_2$ so that only J_2 contributes. From that table it can be seen that this approximation, which has been made throughout this paper, is justified for these compounds. The physical values of the diffusion coefficients and the linewidths were obtained from the dimensionless values by the use of Eq. (14a). The results are summarized in Table X, with the diffusion coefficients quoted

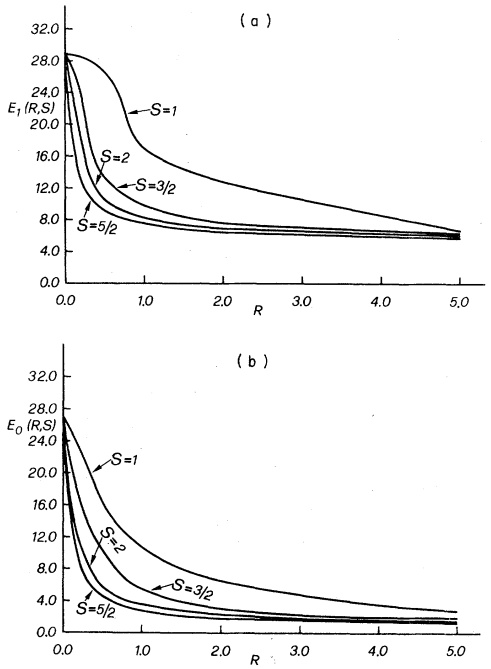

FIG. 10. R- and S-dependent parts of the dipolar linewidths. (a) $E_1(R,S)$; (b) $E_0(R,S)$.

in meV Å^2 and the linewidths quoted in gauss. Also, the second term in Eqs. (23a) and (30a) has been listed in both meV and gauss to aid in the comparison of the magnitudes of first and second terms of those equations. The diffusion coefficients have been computed assuming that $\theta=\frac{1}{2}\pi$ in Eqs. (23) and the notation in the table is the following: $D_1=V\tilde{D}_1$, $D_0=V\tilde{D}_0$, $\Gamma_0^D=V\tilde{\Gamma}_0^D$, $\Gamma_{1b}^D=VRf(S)\tilde{g}_{21}(0)$, and $\Gamma_{1a}^D=V\tilde{\Gamma}_1^D-\Gamma_{1b}^D$, where V is given by $[\frac{16}{3}S(S+1)]^{1/2}J_2$. Finally, it should be noted that the numbers quoted in gauss in Table X depend strongly upon what one chooses for the g value of the ion in question. Since these numbers do not appear to be in the literature for the case where the ions considered here (Ni^{2+}, Co^{2+}, Fe^{2+}, Mn^{2+}) are in the rutile structure, their values in the cubic structure MgO (see Ref. 59) have been used in Table X. Thus, the linewidths quoted in that table could conceivably change considerably

TABLE IX. Summary of relevant data for rutile compounds. All energies are in cm^{-1}. Energies are from Refs. 43–47, lattice constants from Ref. 58.

Compound	Spin	J_1	J_2	J_3	D	a (Å)	c (Å)	R
NiF_2	1	−0.22	13.87	0.79	4.36	4.6506	3.0836	0.0072
CoF_2	$\frac{3}{2}$	−0.83	4.54	0.346	3.53	4.6951	3.1796	0.0299
FeF_2	2	−0.05	3.64	0.19	6.46	4.6966	3.3091	0.0962
MnF_2	$\frac{5}{2}$	−0.44	2.45	0.06	0.74	4.8734	3.3099	0.0019

TABLE X. Spin-diffusion coefficients and dipolar linewidths g values are from Ref. 59.

Compound	D_0 (meV Å^2)	D_1 (meV Å^2)	Γ_{1b}^D (meV)	Γ_0^D (G)	Γ_{1a} (G)	Γ_{1b} (G)	g
NiF_2	19.66	19.86	0.024	28.02	33.97	1907	2.1728
CoF_2	7.97	8.79	0.098	101.29	134.76	7828	2.1705
FeF_2	5.06	7.14	0.408	418.56	717.72	21 280	3.4280
MnF_2	7.92	8.06	0.015	194.11	237.36	1286	2.0014

depending on how the g values of the ions change in going from a cubic to a rutile structure.

From Table X, it can be seen that the spin-diffusion coefficients D_0 and D_1 are within the range of possible observation by present neutron scattering techniques.[60] Furthermore, it is clear that for the compounds listed, the explicitly anisotropy energy-dependent linewidth Γ_{1b}^D is not of sufficient magnitude to totally obscure the observation of D_1 for reasonable values of $|\vec{q}|$. Thus both D_1 and D_0 should be able to be seen in these compounds, although they do not appear to have been measured at the present time in the high-temperature phase where the theory is valid. Such measurements would provide a good test of the present theory.

Also, it can be seen from Table X that, for all compounds shown, the linewidth Γ_0^D is sufficiently small to be resolved by current EPR techniques.[9,13] However, it is also clear from that table that for all compounds shown, the exchange narrowed part of the linewidth $\Gamma_1^D, \Gamma_{1a}^D$, will be totally obscured by the explicitly anisotropy energy-dependent linewidth Γ_{1b}^D and that, furthermore, the total Γ_1^D is probably much too large to be observable in EPR experiments as anything other than a broad background. Thus, it appears as if only Γ_0^D could reasonably be expected to be observable in these compounds.

As far as can be determined, the only compound where such measurements have been made at the high temperatures where this theory is relevant is MnF_2.[9,13] For this compound, Gulley *et al.*[9] find that the room-temperature value of Γ_0^D is 260 ± 10 G. Thus, in comparison with this number, the number obtained from the above infinite-temperature theory (194.1 G) is in error by 25.4%. Considering that the theory is strictly valid only at $T = \infty$ while it is compared to a $T = 300$ K experiment, that the expected error is of the order $1/Z$ or 12.5% for the rutile structure and that Γ_0^D was determined self-consistently, this appears to be a reasonable result. The error here is of the same order of magnitude as that obtained for the isotropic case.[34] On the other hand, Dormann and Jaccarino[13] have more recently measured Γ_0^D for MnF_2 at temperatures up to the melting point. Thus, it is possible to obtain a theoretical-experimental comparison for experimental temperatures of the order 1000 K before the linewidth begins to change drastically as a function of temperature due to the onset of the melting process.[13] (The present rigid lattice model is certainly not valid once this process begins.) Dormann and Jaccarino[13] obtain a Γ_0^D of ~245 G at $T \sim 1073$ K. Thus, comparison of the $T = \infty$ theory to this high-temperature experiment brings the experimental-theoretical discrepancy down to 20%. The measurements of the other linewidths predicted in Table X would be another good test of the theory.

Finally, it should be noted that the numbers for NiF_2 should be treated with caution since there is evidence[43-47] that, for that compound, there is an additional single-ion term in the Hamiltonian of the form $E(S_x^2 - S_y^2)$ which has not been taken into account in the present paper.

VI. SUMMARY AND CONCLUSIONS

In the preceding discussion, a general theory for the first-principles calculation of dynamical two-point spin-correlation functions in a Heisenberg paramagnet with both uniaxial and exchange anisotropy has been presented. By the use of a diagrammatic technique, a set of integral equations for these correlation functions was obtained. These equations are valid at infinite temperature and are applicable at all values of the spin quantum number S and all ratios D/J of the uniaxial anisotropy energy to the exchange energy. Furthermore, these equations form the lowest-order approximation in a heirarchy of the self-consistent approximations which can be generated by carrying the diagrammatic technique to higher-order diagrams. The expected accuracy of the solutions to these equations is of the order of $1/Z$, where Z is the number of spins in the range of the interaction.

In the isotropic exchange limit, the "local" versions of these equations were solved and a study was made of their solutions for $1 \leq S \leq \frac{5}{2}$ and for

various values of R, where R is defined in Eq. (17c). Among other interesting behavior, it was found from these solutions that even for a spin as high as $S=\frac{5}{2}$ one still has not reached the classical limit. In other words, even for $S=\frac{5}{2}$ the solutions, $\tilde{g}_{1m}(y)$, for the local dipolar spectral functions depend strongly on S. The strength of this S dependence, however, varies considerably with the value of R; the classical limit, where $\tilde{g}_{1m}(y)$ would no longer depend on S, is approached faster or large R than for small R.

Using the local dipolar spectral function solutions, $\tilde{g}_{1m}(y)$, approximate wave-vector–dependent linewidth functions $\tilde{\Gamma}_{1m}(\tilde{q},y)$ were generated. From these latter functions the dependence of the spin-diffusion coefficients and the exchange-narrowed dipolar linewidths on R and S were explicitly obtained. It was found that, for these quantities, the classical limit is approached much faster than for the $\tilde{g}_{1m}(y)$, with their S dependences being almost saturated for $S=\frac{5}{2}$. Furthermore, for some values of R and S both spin diffusion and exchange narrowing for $\tilde{g}_{11}(\tilde{q},y)$ are effectively quenched by uniaxial anisotropy effects. Thus it is clear that caution must be used in assuming the classical limit even for systems with S as large as $\frac{5}{2}$, because such an assumption may be valid for some properties of the system and wrong for others.

Finally, the diffusion coefficients and dipolar linewidths for NiF_2, CoF_2, FeF_2, and MnF_2 were calculated. For all four compounds it appears as if both diffusion coefficients (D_1 and D_0) and one of the dipolar linewidths (Γ_0^D) are within observable range by the appropriate experimental techniques. The linewidth Γ_1^D, on the other hand, is too broad to be seen because of uniaxial anisotropy effects. The only experimental number for these compounds which is available for comparison with these calculations appears to be Γ_0^D for MnF_2 and, as is discussed in Sec. V, theory and experiment agree reasonably well for that case.

There are two possible improvements to the present theory which would probably be worthwhile. The first of these is to take into account higher-order diagrams in the self-energy diagrammatic expansion. Fedders[40] has already accomplished a resummation of an infinite subset of these diagrams for the isotropic Heisenberg case and an extension of his formalism to systems with uniaxial anisotropy, although probably a herculean task, might be possible. The second possibility for improving the theory lies in extending it to finite temperatures. Reiter[32,61] has proposed such an extension of the diagrammatic formalism for the isotropic case and perhaps the anisotropic effects considered here could be incorporated into his formalism.

ACKNOWLEDGMENTS

The author would like to thank Professor P. A. Fedders for several discussions and Dr. G. F. Reiter for pointing out Ref. 49 to him and thus helping him find explicit forms for the $C^{20}_{l\pm1,m}$. He is also grateful to Battelle Memorial Institute, Columbus, Ohio, for a two year fellowship during which this work was originated and on whose CDC 6400 computer a portion of the numerical work was done.

APPENDIX A: RELATION BETWEEN THE OPERATORS A_{lm} AND THE RACAH OPERATOR EQUIVALENTS

The irreducible tensor operators A_{lm} and the method of generating them have previously been thoroughly discussed[32,34,48] and they have been listed for $0\leq l\leq 2$ in terms of the ordinary spin operators S_+, S_-, and S_z. Likewise, the Racah operator equivalents $\tilde{O}_{lm}$ have been thoroughly discussed in Ref. 49. In fact, Table I of that reference lists these operators in terms of the ordinary spin operators for $0\leq l\leq 8$. There is a simple one to one relationship between these two kinds of operators which will enable one to conveniently convert the operators $\tilde{O}_{lm}$ in Table I of Ref. 49 into the operators A_{lm} needed in this paper. The relationship can be derived as follows.

Since both the $\tilde{O}_{lm}$ and the A_{lm} are tensor spin operators, there certainly must be a linear relationship between the two for a given S, l, and m. Thus, one can write in general

$$\tilde{O}_{lm}=g(S,l,m)A_{lm}, \tag{A1}$$

where $g(S,l,m)$ is a function to be determined. This function can be determined by taking matrix elements of both sides of Eq. (A1) within a manifold of constant S. Then one has

$$\langle S,m'|\tilde{O}_{lm}|S,\bar{m}\rangle=g(S,l,m)\langle S,m'|A_{lm}|S,\bar{m}\rangle. \tag{A2}$$

The matrix element on the left-hand side of Eq. (A2) has the form[49]

$$\langle S,m'|\tilde{O}_{lm}|S,\bar{m}\rangle=(-1)^{S-m'}\begin{pmatrix} S & l & S\\ -m' & m & \bar{m}\end{pmatrix}\langle S||\tilde{O}_l||S\rangle, \tag{A3}$$

where $\langle S||\tilde{O}_l||S\rangle$ is the reduced matrix element of $\tilde{O}_{lm}$ and

$$\begin{pmatrix} S & l & S\\ -m' & m & \bar{m}\end{pmatrix}$$

is a 3-j symbol. Since A_{lm} is also a tensor operator, the matrix element on the right-hand side of Eq. (A2) must take a similar form[62,63]

$$\langle S,m'|A_{lm}|S,\bar{m}\rangle=(-1)^{S-m'}\begin{pmatrix} S & l & S \\ -m' & m & \bar{m}\end{pmatrix}\langle S||A_l||S\rangle, \tag{A4}$$

where $\langle S||A_l||S\rangle$ is the reduced matrix element of A_{lm}. Comparison of Eqs. (A2)–(A4) leads to the result

$$g(S,l,m)=\langle S||\tilde{O}_l||S\rangle/\langle S||A_l||S\rangle. \tag{A5}$$

Thus $g(S,l,m)$ is independent of m. The reduced matrix element $\langle S||\tilde{O}_l||S\rangle$ is given by[49]

$$\langle S||\tilde{O}_l||S\rangle=\frac{1}{2^l}\left(\frac{(2S+l+1)!}{(2S-l)!}\right)^{1/2}, \tag{A6}$$

while $\langle S||A_l||S\rangle$ is given by[64]

$$\langle S||A_l||S\rangle=[(2S+1)(2l+1)]^{1/2}. \tag{A7}$$

Combining Eqs. (A5)–(A7) and (A1) yields the result

$$\tilde{O}_{lm}=\frac{1}{2^l}\left(\frac{(2S+l+1)!}{(2S-l)!\,(2S+1)(2l+1)}\right)^{1/2}A_{lm}. \tag{A8}$$

Thus, as long as one is working within a manifold of constant S, Eq. (A8) may be used to relate the operators A_{lm} to the $\tilde{O}_{lm}$. Thus, since the $\tilde{O}_{lm}$ are listed in Table I of that reference for $0\leq l\leq 8$, the A_{lm} for those l can be found by the use of that table and Eq. (A8).

APPENDIX B: COMMUTATION PROPERTIES OF THE A_{lm}; EVALUATION OF THE QUANTITIES $C^{lm}_{l,m+m'}$, $C^{20}_{l+1,m}$, AND $C^{20}_{l-1,m}$

From the tensor properties of the A_{lm} it is easily shown that the commutators of Eq. (5) have the forms

$$[A_{1m'},A_{lm}]=C(1m';lm;l,m+m')A_{l,m+m'} \tag{B1}$$

and

$$[A_{20},A_{lm}]=C(20;lm;l-1,m)A_{l-1,m}+C(20;lm;l+1,m)A_{l+1,m}. \tag{B2}$$

As was done in the text, throughout the rest of this appendix the abbreviations

$$C^{1m'}_{l,m+m'}=C(1m';lm;l,m+m') \tag{B3}$$

and

$$C^{20}_{l\pm1,m}=C(20;lm;l\pm1,m) \tag{B4}$$

will be used. The quantity $C^{1m'}_{l,m+m'}$ is trivially calculated from the well-known commutation relations

$$[S_z,A_{lm}]=mA_{lm} \tag{B5}$$

and

$$[S_\pm,A_{lm}]=[l(l+1)-m(m\pm1)]^{1/2}A_{l,m\pm1}, \tag{B6}$$

along with the relations between the A_{1m} and the operators S_z, S_+, and S_-[34]:

$$A_{1,\pm1}=\mp S_\pm/[\tfrac{2}{3}S(S+1)]^{1/2} \tag{B7}$$

and

$$A_{10}=S_z/[\tfrac{1}{3}S(S+1)]^{1/2}. \tag{B8}$$

Combining Eqs. (B5)–(B8) with (B1) yields

$$C^{1,\pm1}_{l,m\pm1}=\mp\left(\frac{3[l(l+1)-m(m\pm1)]}{2S(S+1)}\right)^{1/2} \tag{B9}$$

and

$$C^{10}_{l,m}=[3/S(S+1)]^{1/2}m. \tag{B10}$$

The evaluation of the $C^{20}_{l\pm1,m}$ in closed form is also straightforward although it requires some lengthy algebra. Curiously, although recursion relations between these quantities have been derived and utilized,[64] it appears as if the closed-form expressions for them have never been derived before. The derivation begins with the general commutation relation between two tensor operators, given in Eq. (8) of Ref. 49 for the Racah operators $\tilde{O}_{lm}$. Using that expression along with the results of Appendix A for the relation between the A_{lm} and the $\tilde{O}_{lm}$, one can obtain the general expression

$$[A_{l_1m_1},A_{l_2m_2}]=\sum_{m_3=-l_3}^{l_3}\sum_{l_3=|l_1-l_2|}^{|l_1+l_2|}[(-1)^{l_1+l_2+l_3}-1](2l_3+1)\begin{Bmatrix} l_1 & l_2 & l_3 \\ S & S & S\end{Bmatrix}\begin{pmatrix} l_1 & l_2 & l_3 \\ m_1 & m_2 & m_3\end{pmatrix}\frac{\langle S||A_{l_1}||S\rangle\langle S||A_{l_2}||S\rangle}{\langle S||A_{l_3}||S\rangle}A^\dagger_{l_3m_3}, \tag{B11}$$

where

$$\begin{Bmatrix} l_1 & l_2 & l_3 \\ S & S & S\end{Bmatrix}$$

is a 6-j coefficient,

$$\begin{pmatrix} l_1 & l_2 & l_3 \\ m_1 & m_2 & m_3 \end{pmatrix}$$

is a 3-j coefficient, $\langle S||A_l||S\rangle$ is the reduced matrix element of A_{lm}, and $A^{\dagger}_{l_3 m_3}$ means the Hermitian conjugate of $A_{l_3 m_3}$. Comparison of Eq. (B11) for $l_1 = 2, m_1 = 0$ with Eq. (B2) yields explicit expressions for the $C^{20}_{l\pm1,m}$ which have the form

$$C^{20}_{l-1,m} = (-1)^m[(-1)^{2l+1} - 1](2l-1)\begin{Bmatrix} 2 & l & l-1 \\ S & S & S \end{Bmatrix}\begin{pmatrix} 2 & l & l-1 \\ 0 & m & -m \end{pmatrix}\frac{\langle S||A_2||S\rangle\langle S||A_l||S\rangle}{\langle S||A_{l-1}||S\rangle} \tag{B12}$$

and

$$C^{20}_{l+1,m} = (-1)^m[(-1)^{2l+3} - 1](2l+3)\begin{Bmatrix} 2 & l & l+1 \\ S & S & S \end{Bmatrix}\begin{pmatrix} 2 & l & l+1 \\ 0 & m & -m \end{pmatrix}\frac{\langle S||A_2||S\rangle\langle S||A_l||S\rangle}{\langle S||A_{l+1}||S\rangle} \tag{B13}$$

These expressions can be straightforwardly evaluated, but a considerable amount of algebra is required. The $\langle S||A_l||S\rangle$ can be obtained from Ref. 64 or Eq. (A7) and the 3-j and 6-j symbols can be evaluated by the use of formulas given in any standard text.[65] When Eqs. (B12) and (B13) are evaluated, the results are

$$C^{20}_{l-1,m} = (45)^{1/2}(-1)^{2S}m\left(\frac{(l+m)(l-m)[4S(S+1) - (l-1)(l+1)]}{S(S+1)(2S-1)(2S+3)(2l-1)(2l+1)}\right)^{1/2} \tag{B14}$$

and

$$C^{20}_{l+1,m} = (45)^{1/2}(-1)^{2S}m\left(\frac{(l+m+1)(l-m+1)[4S(S+1) - l(l+2)]}{S(S+1)(2S-1)(2S+3)(2l+1)(2l+3)}\right)^{1/2}. \tag{B15}$$

APPENDIX C: RELATION OF THE $J_{m\,m'}$ OF EQ. (1′) TO THE J_{ab} OF EQ. (1)

To obtain the relationship of the $J_{mm'}$ of Eq. (1′) to the J_{ab} of Eq. (1) one first writes the spin operators S_+, S_-, S_z, and S_z^2 in terms of the tensor spin operators A_{1m} and A_{20}. The relationships for the A_{1m} are given in Eqs. (B7) and (B8) while the relation for A_{20} is[34]

$$A_{20} = [S_z^2 - \tfrac{1}{3}S(S+1)]/\mu_s, \tag{C1}$$

where μ_s is defined in Eq. (1″). Then Eq. (1′) results if the identifications

$$\begin{aligned} &J_{11} = J^*_{-1,1} = \tfrac{1}{2}(J_{xx} - J_{yy} - 2iJ_{xy}), \\ &J_{10} = J_{01} = -J^*_{0,-1} = -J^*_{-1,0} = (J_{xz} - iJ_{yz})/\sqrt{2}, \\ &J_{1,-1} = J_{-1,1} = -(J_{xx} + J_{yy}), \quad J_{00} = J_{zz} \end{aligned} \tag{C2}$$

are made.

*Work supported in part by the Battelle Memorial Institute, Columbus, Ohio.

†Swiss Federal Institute of Technology.

[1]M. E. Lines, Phys. Rev. 156, 534 (1967).
[2]T. Murao and T. Matsubara, J. Phys. Soc. Jpn. 25, 352 (1968).
[3]J. F. Devlin, Phys. Rev. B 4, 136 (1971).
[4]M. Tanaka and Y. Kondo, Prog. Theor. Phys. 48, 1815 (1972).
[5]N. A. Potapkov, Theor. Mat. Fiz. 8, 381 (1971).
[6]S. B. Haley and P. Erdos, Phys. Rev. B 5, 1106 (1972).
[7]C. Vettier, J. Phys. C 7, 3583 (1974).
[8]M. E. Lines, Phys. Rev. B 12, 3766 (1975).
[9]J. E. Gulley, D. Hone, D. J. Scalapino, and B. G. Silbernagel, Phys. Rev. B 1, 1020 (1970).
[10]M. S. Seehra and T. G. Castner, Solid State Commun. 8, 787 (1970).
[11]M. S. Seehra, J. Appl. Phys. 42, 1290 (1971).
[12]M. S. Seehra, Phys. Rev. B 6, 3186 (1972).
[13]E. Dormann and V. Jaccarino, A.I.P. Conf. Proc. 18, 529 (1973).
[14]C. R. Natoli and J. Ranninger, J. Phys. C 6, 345 (1973).
[15]C. R. Natoli and J. Ranninger, J. Phys. C 6, 370 (1973).
[16]M. T. Hutchings, Phys. Rev. B 5, 154 (1972).
[17]R. A. Cowley, W. J. L. Buyers, P. Martel, and R. W. Stevenson, J. Phys. C 6, 2997 (1973).
[18]Examples of real magnetic insulators with uniaxial anisotropy are NiF_2, CoF_2, FeF_2, and MnF_2.
[19]R. C. Richardson, E. Hunt, and H. Meyer, Phys. Rev. 138, A1326 (1965).
[20]A. B. Harris, Solid State Commun. 9, 2255 (1971).
[21]W. C. Thomlinson, J. F. Kelly, and R. C. Richardson, Phys. Lett. A 38, 531 (1972).
[22]D. L. Huber, Phys. Rev. B 6, 3180 (1972).
[23]D. L. Huber, M. S. Seehra, and P. W. Verbeek, Phys. Rev. B 9, 4988 (1974).
[24]B. I. Halperin, P. C. Hohenberg, and S. K. Ma, Phys. Rev. B 10, 139 (1974).
[25]R. B. Woolsey, and R. M. White, Int. J. Magn. 2, 51

(1972).
[26]A. B. Harris, D. Kumar, B. I. Halperin, and P. C. Hohenberg, Phys. Rev. B 3, 961 (1971).
[27]R. M. White, R. Freedman, and R. B. Woolsey, Phys. Rev. B 10, 1039 (1974).
[28]F. A. Malinoski, Phys. Rev. B 8, 1170 (1973), and references therein.
[29]C. Joukoff-Piette and P. Resibois, Physica 63, 425 (1973).
[30]P. Resibois and C. Joukoff-Piette, Physica 63, 459 (1973).
[31]P. Resibois and M. Deleener, Phys. Rev. 152, 305 (1966); 152, 318 (1966); 178, 806 (1969); 178, 869 (1969).
[32]G. F. Reiter, Phys. Rev. B 5, 222 (1972).
[33]H. S. Bennett and P. C. Martin, Phys. Rev. 138, A608 (1965).
[34]C. W. Myles and P. A. Fedders, Phys. Rev. B 9, 4872 (1974).
[35]C. W. Myles, Phys. Rev. B 11, 3225 (1975); 11, 3238 (1975).
[36]C. W. Myles and C. Ebner, Phys. Rev. B 11, 2339 (1975); 12, 1608 (1975).
[37]P. A. Fedders, C. W. Myles, and C. Ebner, A.I.P. Conf. Proc. 24, 338 (1975).
[38]C. W. Myles, C. Ebner, and P. A. Fedders, Phys. Rev. B 14, 1 (1976).
[39]C. W. Myles, Phys. Rev. B 13, 3199 (1976).
[40]P. A. Fedders, Phys. Rev. B 12, 3933 (1975).
[41]R. B. Stinchcombe, G. Horwitz, F. Englert, and R. Brout, Phys. Rev. 130, 185 (1963).
[42]V. G. Vaks, A. I. Larkin, and S. A. Pikin, Sov. Phys.-JETP 26, 188 (1968); 26, 647 (1968).
[43]N. A. Begum, A. P. Cracknell, S. J. Joshva, and J. A. Russland, J. Phys. C 2, 2329 (1969).
[44]O. Nickotin, P. A. Lindgärd, and O. W. Deutsch, J. Phys. C 2, 1168 (1969).
[45]M. T. Hutchings, M. F. Thorpe, R. J. Birgeneau, P. S. Fleury, and H. J. Guggenheim, Phys. Rev. B 2, 1362 (1970).
[46]S. J. Joshova and A. P. Craknell, J. Phys. C 2, 24 (1969).
[47]M. T. Hutchings, B. D. Rainford, and H. J. Guggenheim, J. Phys. C 3, 307 (1970).
[48]C. W. Myles, Ph.D. thesis (Washington University, St. Louis, Mo., 1973) (unpublished).
[49]P. A. Lingärd and O. Danielsen, J. Phys. C 7, 1523 (1974).
[50]See, for example, A. A. Abrikosov, L. P. Gorkov, and Ye. Dzyaloshinskii, *Quantum Theoretical Methods in Statistical Physics* (Pergamon, New York, 1965).
[51]P. A. Fedders, Phys. Rev. B 3, 2352 (1971).
[52]M. Blume and J. Hubbard, Phys. Rev. B 1, 3815 (1970).
[53]H. S. Bennett and E. Pytte, Phys. Rev. 155, 553 (1967).
[54]L. P. Kadanoff and P. C. Martin, Ann. Phys. (N.Y.) 24, 419 (1963).
[55]J. H. Vleck, Phys. Rev. 74, 1169 (1948).
[56]P. W. Anderson and P. R. Weiss, Rev. Mod. Phys. 25, 269 (1953).
[57]R. Kubo and K. Tomito, J. Phys. Soc. Jpn. 9, 888 (1954).
[58]R. W. Wyckoff, *Crystal Structure* (Wiley, New York, 1963), Vol. 1, p. 251.
[59]A. Abragam and B. Bleaney, *Electron Paramagnetic Resonance of Transition Ions* (Oxford, University, London, 1970).
[60]A. Tucciarone, J. M. Hastings, and L. M. Corliss, Phys. Rev. Lett. 26, 252 (1971); Phys. Rev. B 8, 1103 (1973).
[61]G. F. Reiter, Phys. Rev. B 7, 3325 (1973).
[62]G. Racah, Phys. Rev. 62, 438 (1942).
[63]See, for example, K. Gottfried, *Quantum Mechanics* (Benjamin, New York, 1966), Vol. 1, p. 302.
[64]P. A. Fedders, Phys. Rev. B 11, 995 (1975).
[65]See, for example, M. Tinkham, *Group Theory and Quantum Mechanics* (McGraw-Hill, New York, 1964), Chap. 5.